Investigating the kinematics of mountain building in Taiwan from the spatiotemporal evolution of the foreland basin and western foothills

Martine Simoes, Jean-Philippe Avouac

Investigating the kinematics of mountain building in Taiwan from the spatiotemporal evolution of the foreland basin and western foothills

Martine Simoes[1,2,3] and Jean Philippe Avouac[1]

Received 8 December 2005; revised 7 June 2006; accepted 23 June 2006; published 5 October 2006.

[1] The Taiwanese range has resulted from the collision between the Luzon volcanic arc and the Chinese continental margin, which started about 6.5 Myr ago in the north, and has since propagated southward. The building of the range has been recorded in the spatiotemporal evolution of the foreland basin. We analyze this sedimentary record to place some constraints on the kinematics of crustal deformation. The flexure of the foreland under the load of the growing wedge started with a 1.5 Myr long phase of rapid subsidence and sedimentation, which has migrated southward over the last 3.5 Myr at a rate of 31 +10/−5 mm/yr, reflecting the structural evolution of the range and the growth of the topography during the oblique collision. Isopachs from the Toukoshan (∼0 to 1.1 Ma) and Cholan (∼1.1 to 3.3 Ma) formations, as well as the sedimentation rates retrieved from a well on the Pakuashan anticline, indicate that the foreland basement has been moving toward the center of mass of the orogen by ∼45–50 mm/yr during the development of the basin. From there, we estimate the long-term shortening rate across the range to 39.5–44.5 mm/yr. By considering available data on the thrust faults of the foothills of central Taiwan, we show that most (if not all) the shortening across the range is accommodated by the most frontal structures, with little if any internal shortening within the wedge. The range growth appears therefore to have been essentially sustained by underplating rather than by frontal accretion. In addition, only the upper ∼7 to 9 km of the underthrusted crust participates to the growth of the orogen. This requires that a significant amount of the Chinese passive margin crust is subducted beneath the Philippine Sea plate.

Citation: Simoes, M., and J. P. Avouac (2006), Investigating the kinematics of mountain building in Taiwan from the spatiotemporal evolution of the foreland basin and western foothills, *J. Geophys. Res.*, *111*, B10401, doi:10.1029/2005JB004209.

1. Introduction

[2] In this paper, we describe how the kinematics of an orogenic wedge (Figure 1), which evolves under the effect of crustal shortening, accretion and erosion [e.g., *Avouac*, 2003; *DeCelles and DeCelles*, 2001; *Whipple and Meade*, 2006], can be determined from the history of sedimentation in the foreland and from the development of the foothills fold-and-thrust belt system. We focus here on Taiwan. This young orogeny, which has resulted from the collision between the Luzon arc and the Chinese continental margin (Figure 2), has been extensively studied in the past and has been key to the development of the popular critical wedge model of mountain building [*Barr and Dahlen*, 1989; *Barr et al.*, 1991; *Dahlen and Barr*, 1989; *Davis et al.*, 1983; *Suppe*, 1981]. However, some first-order kinematic parameters, such as the long-term shortening as well as how it is distributed across the range, are still not yet resolved to test the model. Because of the obliquity between the Chinese passive margin and the Luzon Volcanic Arc, the collision is propagating southward [*Suppe*, 1981] (Figure 2), so that the temporal evolution of mountain building might be retrieved by analyzing transects at different latitudes across the range. However, the rate of collision propagation is still not well constrained, and proposed values range from 55 to 90 mm/yr [*Byrne and Liu*, 2002; *Liu et al.*, 2001; *Suppe*, 1981, 1984]. The kinematics of deformation and of mountain building in Taiwan might be quantified better from the analysis of the spatiotemporal evolution of the foreland basin and western foothills system. Indeed, foreland basins develop by flexure under the load of a migrating orogen [*Beaumont*, 1981; *Jordan*, 1981] and are filled by the sediments derived from the eroding mountain belt. As such, they record the evolution of the prograding range, in their stratigraphic architecture and subsidence history [e.g., *Avouac*, 2003; *Lyon-Caen and Molnar*, 1985]. In the case of Taiwan, seismic profiles and well logs across the foreland, as well as across the accreted synorogenic sediments of the

[1]Tectonics Observatory, California Institute of Technology, Pasadena, California, USA.
[2]Laboratoire de Géologie, CNRS Ecole Normale Supérieure, Paris, France.
[3]Now at Géosciences Rennes, CNRS Université Rennes 1, Rennes, France.

0148-0227/06/2005JB004209$09.00

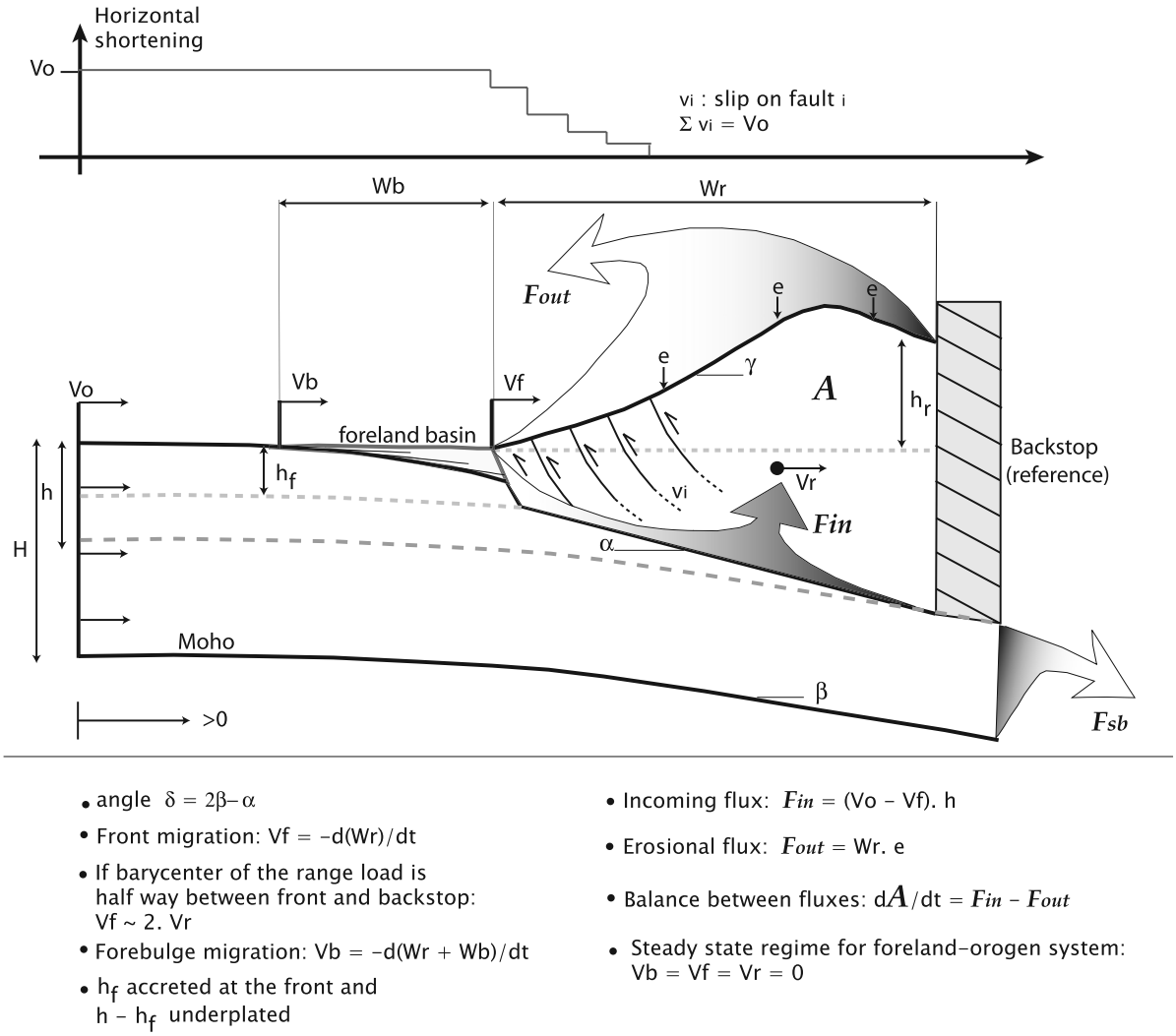

Figure 1. Schematic diagram defining the kinematic framework used for this study. All velocities are relative to the backstop and taken positive toward the backstop. See text for further details.

foothills, conducted since the 1960s for oil exploration [e.g., *Covey*, 1984a, 1986; *Lin et al.*, 2003; *Yu and Chou*, 2001], document quite extensively the development of the basin and its interaction with the adjacent mountain belt. In this study, we use these data to derive the southward propagation of the range growth in Taiwan, the westward progradation rate of the orogen over its basin, and from there the long-term shortening rate across the range.

2. Principles of Our Kinematic Analysis

[3] The principle of our kinematic analysis is schematically illustrated on Figure 1. The backstop of the range, defined as the undeformed area at the back of the orogen-foreland system, is taken as the fixed reference; velocities are considered positive toward the range (from left to right on Figure 2). The distant nondeformed footwall, of total crustal thickness H, is moving toward the backstop at a velocity V_o, equal to the total rate of shortening absorbed across the range, as a result of shortening v_i across each of the various faults i. As it encounters the orogenic belt, a crustal slice of the footwall with a thickness h (with $h \leq H$) is incorporated into the range by frontal accretion and/or underplating, and gets to be deformed. The model allows for some crustal subduction represented by the outgoing flux F_{sb}. The orogen is allowed to deform in order to adjust to the incoming flux of rocks F_{in} as well as to long-term erosion e averaged over the whole mountain belt. If the incoming flux exceeds the outcoming flux, then the orogenic prism grows and widens: the topographic front of the range moves away from the backstop at a velocity V_f (negative according to our sign convention, Figure 1), and the center of mass of the whole range moves at a rate V_r (also negative). Similarly, if the prism shortens because the eroding flux F_{out} exceeds accretion and underplating, V_r and V_f will be directed toward the backstop and will thus be positive. In the case of a steady prism, these migration rates of the front and of the load of the range would equal zero (Figure 1). If we assume that the center of mass of the range load approximately stands about midway between the front and the backstop, we have $V_f \sim 2\ V_r$. The load of the range

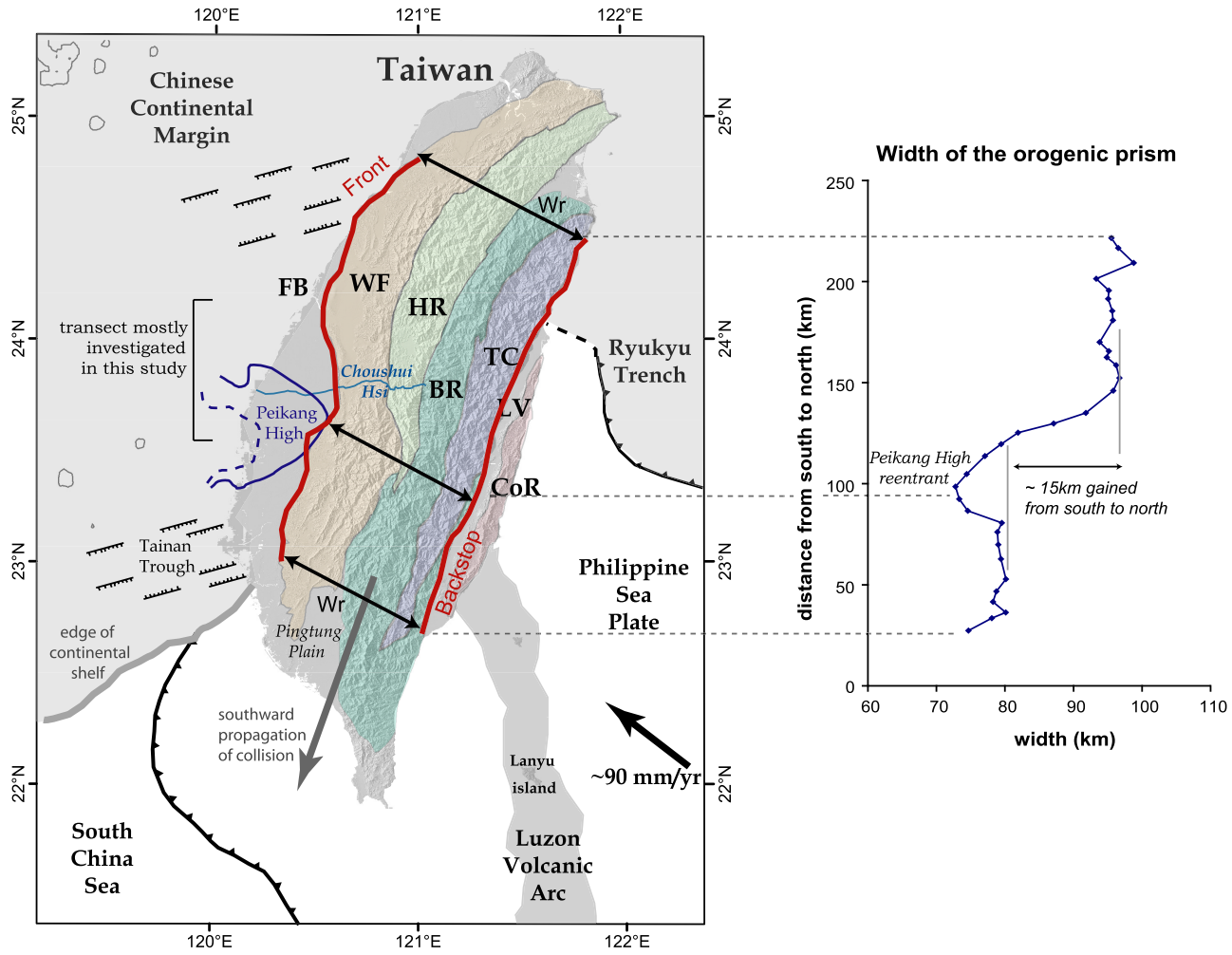

Figure 2. (left) Geodynamical setting of the arc-continent collision of Taiwan showing the two plates and the two subduction zones of reverse polarities. Thick arrow shows the convergence of the Philippine Sea Plate relative to the Chinese Continental Margin predicted from the global plate geodetic model REVEL [*Sella et al.*, 2002]. Also reported are the location of the main structural units of Taiwan: CoR, Coastal Range; LV, Longitudinal Valley; TC, Tananao Complex; BR, Backbone Range; HR, Hsueshan Range; WF, Western Foothills; FB, Foreland Basin. The east-west geometry of the Peikang Basement High is indicated by the 2 km (continuous line) and 1 km (dashed line) contours of Cenozoic sediment thicknesses taken after *Lin et al.* [2003]. (right) Lateral variations of the range width, and reentrant observed in central Taiwan, related to the indenting Peikang high.

is responsible for the flexural foreland basin, so that the forebulge migration rate V_b should also reflect the growth of the orogenic prism.

[4] In a two-dimensional (2-D) view, the cross-sectional area A of the orogenic belt can be approximated by relating the dip angles α and β of the basal decollement and of the underthrusted Moho, respectively, the thickness h of the accreted slice of footwall crust, the range width W_r and the range topography h_r:

$$A \approx W_r\left(h + \frac{h_r}{2} + \frac{1}{2}W_r \tan\delta\right) \tag{1}$$

where $\delta = 2\beta - \alpha$. This approximation is valid if dip angles are not too large so that $\tan(\beta) \cdot \tan(\delta) \ll 1$. Variation in time of A depends on how incoming F_{in} and eroding fluxes F_{out} balance each other:

$$\frac{dA}{dt} = F_{in} - F_{out} = h \cdot \left(V_0 + \frac{dw}{dt}\right) - e \cdot w \tag{2}$$

We may suppose that the prism grows or shortens self-similarly in time, as in the case of a critical wedge and thus that the taper angle $\gamma + \alpha$ (where γ is the topographic slope) does not vary. If we infer that the thickness h of the crustal slice accreted and/or underplated to the orogenic belt is

constant over time, the only time variable of equation (1) is the width of the range $W_r(t)$. The analytical solution of equation (2) relating W_r and time t is

$$t = t_0 - a \cdot [W_r(t) - W_r(t_0)] - a \cdot W_c \cdot \ln\left(\frac{W_c - W_r(t)}{W_c - W_r(t_0)}\right) \quad (3)$$

where

$$a = \frac{\tan(\delta) + \tan(\gamma)}{e}$$

The parameter

$$W_c = \frac{V_0 \cdot h}{e}$$

represents the asymptotic value of $W_r(t)$ expected for a system that has reached a steady state regime in which incoming and outcoming fluxes balance each other.

3. Structural Framework, Stratigraphy and Architecture of the Foreland Basin

3.1. Structural Framework

[5] Taiwan has resulted from the collision between the Luzon Volcanic Arc and the Chinese continental margin (Figure 2), ~6.5 Myr ago to the north of the island, as inferred from the age of the recorded foreland unconformity [*Lin et al.*, 2003]. Because of the obliquity between the directions of these structures, the collision has propagated southward along the island, at probable rates of ~55 to 90 mm/yr inferred from the present geometries of the arc and of the margin offshore southwestern Taiwan [*Byrne and Liu*, 2002; *Suppe*, 1981, 1984] (Figure 2).

[6] To the east, the rocks forming the Coastal Range, CoR, and the Longitudinal Valley, LV, have geologic affinities with the Luzon arc while those within the Central Range (CR), west of the LV have affinities with the Chinese continental margin [e.g., *Ho*, 1986, 1988] (Figure 2). In addition, the CoR has not undergone any significant crustal thickening [*Hetland and Wu*, 1998; *Shih et al.*, 1998; *Yeh et al.*, 1998], so that long-term deformation of this unit has been limited. The LV and CoR (Figure 2) are therefore considered to form the backstop of our kinematic model (Figure 1). The shortening rate across the Taiwan range V_o has been previously estimated to ~27 to 45 mm/yr based on geodetic modeling [*Dominguez et al.*, 2003; *Hsu et al.*, 2003; *Loevenbruck et al.*, 2001; *Yu et al.*, 1997]. However, it is not obvious that this short-term value is representative of the long-term rate. The deformation front to the west, which corresponds to the edge of the fold-and-thrust belt of the Western Foothills (WF), marks the frontal limit of the mountain system modeled in Figure 1. The width W_r of the orogenic belt is thus defined from the LV to the westernmost extent of the WF. The lateral variation of W_r is interpreted to reflect the time evolution of the width of the orogenic prism $W_r(t)$ as expressed in equation (3) (Figure 2). To the north of Taiwan, interaction between the mountain belt and the Ryukyu trough is responsible for the more easterly trend of the structures [*Suppe*, 1984] and for the fading of the range [e.g., *Liu et al.*, 2001]. Since our study deals with the orogenic phase, we only focus on the region south of ~ 24°30′N where collision is ongoing and thought to be mature [*Shyu et al.*, 2005]. We consider sections across the range in a N110°E direction, perpendicular to the main N20°E structural trend of the orogen (Figure 2).

[7] The Chinese margin shows lateral complexities due to basins and horsts formed during a phase of extension prior to the current collisional regime [e.g., *Lin et al.*, 2003; *Teng et al.*, 1991]. One of these structures, the Peikang High offshore west central Taiwan [e.g., *Cheng et al.*, 2003; *Hsu and Sibuet*, 1995; *Lin et al.*, 2003], is believed to be responsible for the arcuate geometry of the range front in this region [*Mouthereau et al.*, 1999] (Figure 2).

3.2. Stratigraphy of the Foreland Basin

[8] Synorogenic sediments have been deposited in the foreland basin, and subsequently scrapped off and incorporated into the WF by the westward encroaching orogen. The ages of the synorogenic deposits were inferred mainly from the analyses of calcareous nannoplankton [*Chang and Chi*, 1983; *Chi and Huang*, 1981] and plankton foraminifera [*Huang*, 1984], and were calibrated by magnetostratigraphy [*Horng and Shea*, 1996]. From older to younger levels, they form the Kueichulin, Chinshui, Cholan and Toukoshan formations (Table 1). The Late Miocene Kueichulin Formation, which started depositing ~ 6.5 Myr ago [*Lin et al.*, 2003], is essentially composed of sandstones intercalated with sandy shales. This unit marks the onset of synorogenic deposit since it caps the regional basal foreland unconformity. It is conformably overlain by the Pliocene shales and siltstones forming the Chinshui Shale. The transition between these two sedimentary formations is dated to ~3.6 Ma since it occurs shortly after the NN15-NN16 nannobiostratigraphical transition [*Chi and Huang*, 1981; *Lin et al.*, 2003; *Teng*, 1987]. The Chinshui Shale is overlain by the Upper Pliocene Cholan Formation. Light gray to brownish shales, intercalated with fine to coarse sandy layers, are the major component of this level. Deposition of the Cholan Formation started by ~3.3 Ma [*Chang and Chi*, 1983; *Chen et al.*, 2001] before giving way, by ~1.1 Ma [*Chang and Chi*, 1983; *Chen et al.*, 2001; *Chi and Huang*, 1981; *Covey*, 1984a, 1984b; *Horng and Shea*, 1996], to the Pleistocene sequence of the Toukoshan Formation. Sandy alluvial sequences are rapidly overlain by poorly sorted coarser sediments, mostly conglomerate river assemblages including sandstone lenses. The depositional environments of these synorogenic strata altogether show an overall shallowing and coarsening upward trend, from distal to proximal facies, illustrating the westward progradation of the orogenic belt [*Covey*, 1984a].

3.3. Structure and Time Evolution of the Foreland Basin

[9] The spatiotemporal distribution of lithofacies in the synorogenic sediments of the Coastal Plain and the WF indicates that the foredeep has evolved from an earlier underfilled stage characterized by low sedimentation rates and deep marine deposits, to an overfilled and most probable steady state stage with mostly fluvial or shallow marine sediments [*Covey*, 1984a, 1984b, 1986]. Transient high sedimentation rates would take place during the transition

Table 1. Ages and General Description of the Synorogenic Deposits[a]

Formation	Simplified Description	Age, Ma
Toukoshan	fluvial sands and conglomerates	0 to 1.1
Cholan	shales intercaled with sands	1.1 to 3.3
Chinshui	shales and siltstones	3.3 to 3.6
Kueichulin	sandstones and shales	3.6 to 6.5

[a]See text for details.

from these two stages, in order to fill the space created by the load of the growing orogen and by the increasing amount of sediments delivered to the basin. This temporal evolution can be also presently observed along strike, since the northern basin has already attained a steady overfilled geometry, while to the south deep offshore marine sediments are still present within the foreland [*Covey*, 1986]. As for central Taiwan, shallow marine deposits have prevailed over the last $\sim$ 0.45 Myr indicating that the basin has reached a steady state in this region only recently. *Covey* [1984a, 1984b, 1986] noticed the upward coarsening of the

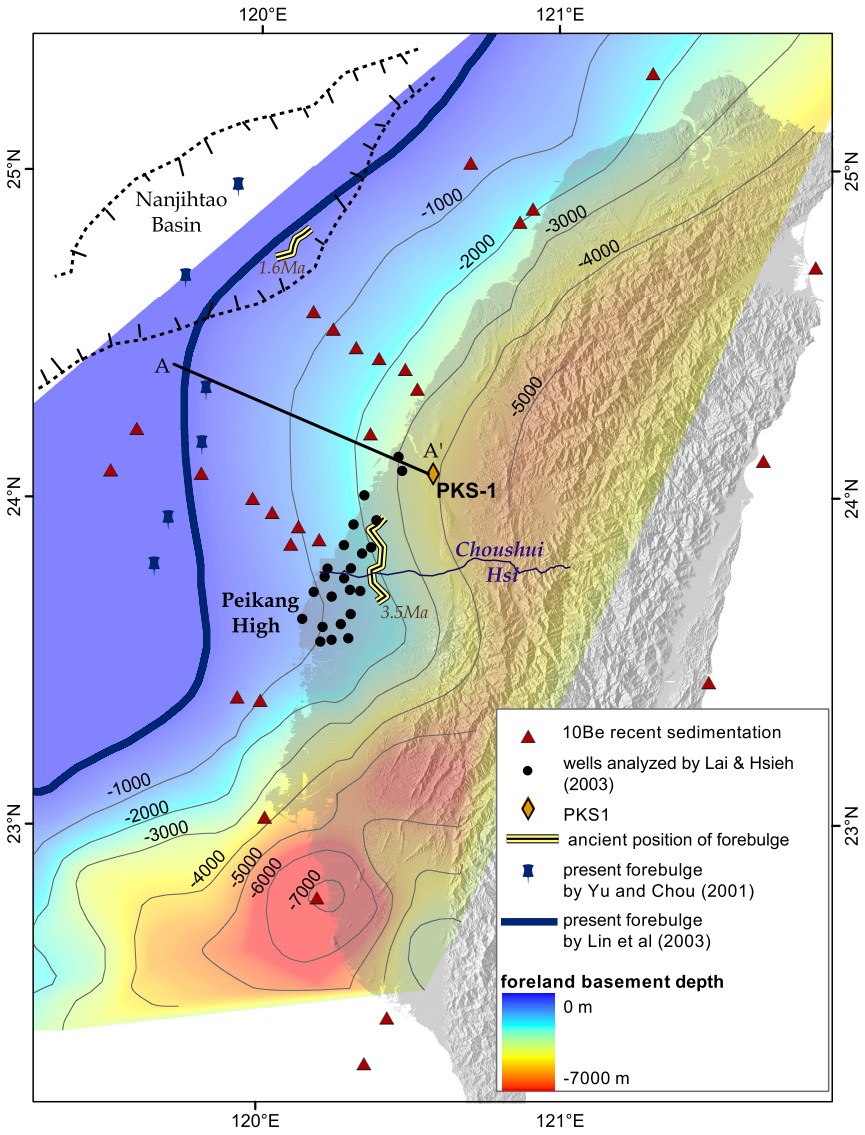

Figure 3. Map view of the data used to investigate the foreland basin of Taiwan. The geometry of the basal foreland unconformity (contours and color) has been retrieved by *Lin et al.* [2003] from the analysis of seismic lines and wells within the Taiwan Strait. Proposed present positions of the forebulge [*Lin et al.*, 2003; *Yu and Chou*, 2001] may be questionable because they might not be easily retrieved in complex areas such as within the Nanjihtao basin. The position of ancient bulges have been estimated from onlapping features (1.6 Ma [*Yu and Chou*, 2001]) or from the boundary separating sediments of mainland China and Taiwan affinities (3.5 Ma [*Covey*, 1984a, 1984b]); the ages of this bulges are here given after the paleomagnetic calibration of *Horng and Shea* [1996]. *Lai and Hsieh* [2003] estimated recent subsidence rates. Recent sedimentation rates from *Lee et al.* [1993] are derived from ^{10}Be content. We mainly analyze the foreland basin along transect A-A′, west of central Taiwan.

synorogenic sediments and related it to a probable record of the westward progradation of the orogen over the foreland. The possible location of a 3.5 Myr old forebulge in central Taiwan was inferred on the basis of sediment provenance within three wells of central Taiwan [*Covey*, 1986] (Figure 3). A detailed age analysis of the PKS-1 well (Figure 3) based on nannobiostratigraphy [*Covey*, 1984b] has been interpreted in terms of sedimentation rates by M. Simoes et al. (Kinematic analysis of the Pakuashan fault-tip fold, west central Taiwan: Shortening rate and age of folding inception, submitted to *Journal of Geophysical Research*, 2005, hereinafter referred to as Simoes et al., submitted manuscript, 2005), after decompaction based on *Audet*'s [1995] law and using the parameters from the Taihsi Basin [*Lin et al.*, 2003].

[10] Offshore well data along with seismic investigations within the Taiwan Strait (Figure 4) allowed for recognizing and mapping a regional foreland basal unconformity with onlapping features and westward increasing sedimentary gap, as well as the eventual position of the present forebulge [*Lin et al.*, 2003; *Yu and Chou*, 2001] (Figure 3). A smoothed interpolated geometry of the flexed foreland basement is accessible from *Lin et al.*'s [2003] study (Figure 3). The inferred present position of the forebulge lies at the westward limit of the seismic lines and well coverage over north and central Taiwan (Figure 4) so that it is probably an easternmost limit for its actual position. Moreover, young orogen-parallel normal faults within the basin, probably due to inelastic yielding of the foreland basement [*Chou and Yu*, 2002], make the determination of the forebulge quite uncertain. Thicknesses of the different synorogenic formations preserved in the basin of north and central Taiwan and of their temporally correlated southern equivalents have been derived by *Shaw* [1996] from offshore and onshore wells (Figures 5a–5d). These wells cover most of the foreland basin (Figure 4), from north to as south as offshore Tainan, but do not document the sediments immediately south of Kaohsiung. Note that in *Shaw*'s [1996] study these synorogenic formations were defined and spatially correlated through the time interval that they represent rather than through their sedimentary facies. Also, only interpolated and spatially smoothed thicknesses are accessible from [*Shaw*, 1996] (Figures 5a–5d). Onland data have to be considered with caution since they have not been corrected for westward tectonic transport and eventual thickening associated with deformation in the fold-and-thrust belt of northern Taiwan. We checked that the cumulated thicknesses of the synorogenic sediments derived by *Shaw* [1996] were compatible with the depth to the foreland basement proposed by *Lin et al.* [2003]. Only some slight discrepancies are observed in northern Taiwan, most probably because of shortening of the sedimentary layers. Subsidence of the Coastal Plain in western Taiwan is documented over the Holocene by *Lai and Hsieh* [2003] (Figure 3). In addition to that, ^{10}Be contents of sediments younger than 3 to 4 ka across the Taiwan Strait allowed for retrieving recent sedimentation rates [*Lee et al.*, 1993] (Figure 3), which show their highest values southward from offshore the mouth of the Choushui Hsi, one of the biggest rivers of the island (Figure 2). Such repartition is comparable to coastal sediment fluxes derived by *Dadson et al.* [2003] over much shorter timescales of $\sim$ 30 years. Southward transport of sediments is presently observed [e.g., *Dadson et al.*, 2003].

4. Analysis of the Spatiotemporal Evolution of the Foreland Basin

4.1. Southward Propagation of Foreland Subsidence and of Orogenic Growth

[11] The isopach maps of the Kueichulin, Chinshui, Cholan and Toukoshan formations [*Shaw*, 1996] show a systemic pattern of southward migration. In Figures 5a–5d, we mapped the area where preserved sediment thickness exceeds 90% of the maximum observed value. These areas probably represent well the original depot centers in the case of the Toukoshan and Cholan formations which are the youngest and best preserved formations. For the older formations, they only provide an estimate of the along-strike position of past depot centers since they have probably been accreted to the foothills and even eroded away. A clear southward propagation of depot centers from Chinshui to Toukoshan formations is observed (Figure 5e). The Kueichulin Formation does not fit into this continuous trend indicating that such southward migration rate has varied over time. However, this can also be an artifact from the scarcity of well data offshore northwestern Taiwan in *Shaw*'s [1996] study (Figure 4). Although the location of greatest sedimentation propagated to the south over time, deposition still persists laterally to the north but not to the south, most probably because the Peikang High has obstructed southward transport of sediments (Figures 5a, 5b, 5c, and 5d). This suggests that, along a transect, this migrating localized zones of high sedimentation rates are only transient. As initially proposed by *Covey* [1986], the high sedimentation rates probably correspond to the early stage of development and filling of the foreland basin until it approaches a steady overfilled stage. Taking into account the ages of the different sedimentary formations (Table 1), and from the position of the centroids of the retrieved depot centers along a N20E direction (Figure 5e), a southward propagation rate of 31 +10/−5 mm/yr is derived (lower inset in Figure 5e) from Chinshui to Toukoshan times. The uncertainty on this estimate accounts for the range of ages assigned to the various formations, and does not explicitly account for the uncertainties on the geometries of the depot centers. Assuming that this rate can be extrapolated up to the present, the area with high subsidence rates corresponding to the filling of the basin would be located $\sim$17 km south of the Toukoshan depot center, at the mouth of the Choushui river (Figure 5e). This is consistent with the high sedimentation rates observed in this area [*Lee et al.*, 1993] and further south [*Dadson et al.*, 2003; *Lee et al.*, 1993]. These results based on sediment thicknesses are also consistent with the analysis of lithofacies by *Covey* [1986], in which the foreland basin south of the Choushui river is still presently underfilled in contrast to the more mature stages observed to the north.

[12] We interpret the southward migrating depot centers as reflecting a propagating flexural signal related to the load of the growing orogen and of the deposited sedimentary piles. Sediments delivered to the basin are expected to fill up first the space created by flexure under the range load immediately offshore the growing topography. Lateral trans-

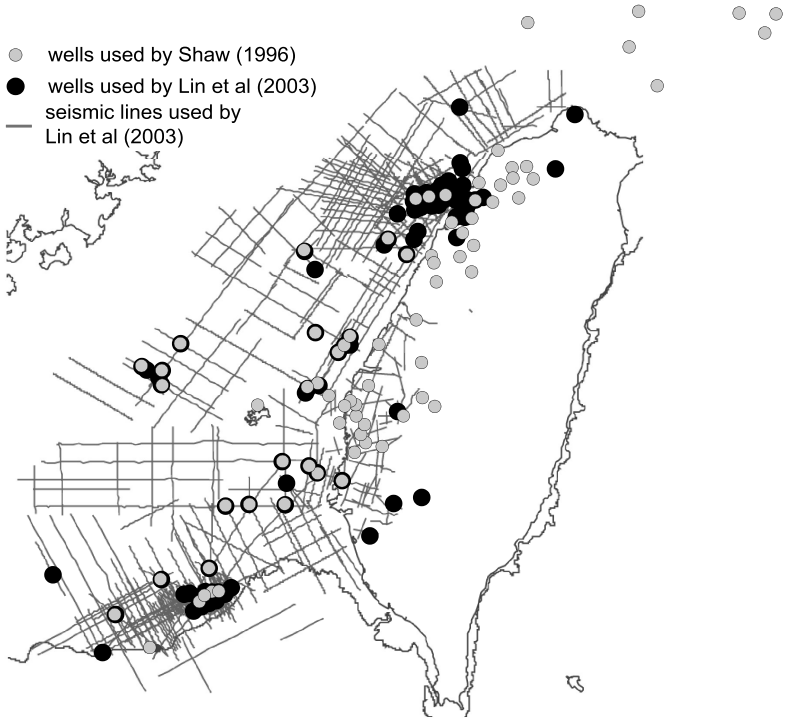

Figure 4. Seismic lines and well coverage used in the study of *Lin et al.* [2003] to define the geometry of the foreland basement shown on Figure 3. The isopach maps of the synorogenic sediments of Figure 5 were derived by *Shaw* [1996] essentially based on well logs. In any case the total foreland thicknesses by *Shaw* [1996] were consistent with the depth to basement proposed by *Lin et al.* [2003].

port within the foreland, controlled by the complex architecture of the margin, would simply redistribute the excess volume. The amplitude of the flexural response of the basin is expected to vary laterally between different transects as the mechanical properties of the foreland certainly depend on the structure of the margin. Also, such amplitude is also controlled by the total amount of sediments delivered to the basin, and thus by temporal changes in climate-driven erosion over the whole island at a given time. Given all these considerations, the retrieved 31 +10/−5 mm/yr migration of the depot centers (Figure 5e) simply mirrors the southward propagation of the orogen. This rate is quite lower than estimates based on the plate convergence rate and on the obliquity between the Luzon Arc and the Chinese continental margin, which range between ~55 and 90 mm/yr [*Byrne and Liu*, 2002; *Suppe*, 1981, 1984]. Hereafter, we use our estimate to relate the temporal evolution and the lateral variations of the range.

4.2. Westward Progradation of the Orogen Over the Foreland Basin

4.2.1. Forebulge Migration

[13] We focus here on a transect across the foreland basin (A-A′ in Figures 3 and 5e) to gain insights into the eastward motion of the basin toward the range. In the case of filled to overfilled basins, sediments prograde up to the forebulge and/or overpass it. The past position of the bulge within the basin might be derived from the onlapping stratigraphy (Figure 6). The migration rate of the bulge corresponds to the differential velocity $V_o - V_b$ with respect to the backstop

Figure 5. Southward propagation of the foreland basin depot centers in time. (a–d) Preserved synorogenic sediment thicknesses of *Shaw* [1996] for different periods of time, from 6.5 Ma to recent times. Names of the formations are given after the terminology used for north and central Taiwan, and represent time intervals rather than sedimentary facies. The respective depot centers are highlighted by a black line. (e) Comparison of the different synorogenic depot centers retrieved in Figures 5a–5d, which show a clear southward migration. The area where current sedimentation is maximum would be at the latitude and south of the Choushui Hsi river, which is consistent with the Holocene measurements of *Lee et al.* [1993]. Contours of the basement depth [*Lin et al.*, 2003] shown in Figure 3 are also reported. Lower inset shows southward migration rate of preserved synorogenic depot centers constrained to 31 +10/−5 mm/yr based on the ages of the sediments (Table 1). Upper inset shows predicted geometry of the underthrusted margin that would fit the total convergence rate of 90 mm/yr and a 31 mm/yr southward propagation of the collision.

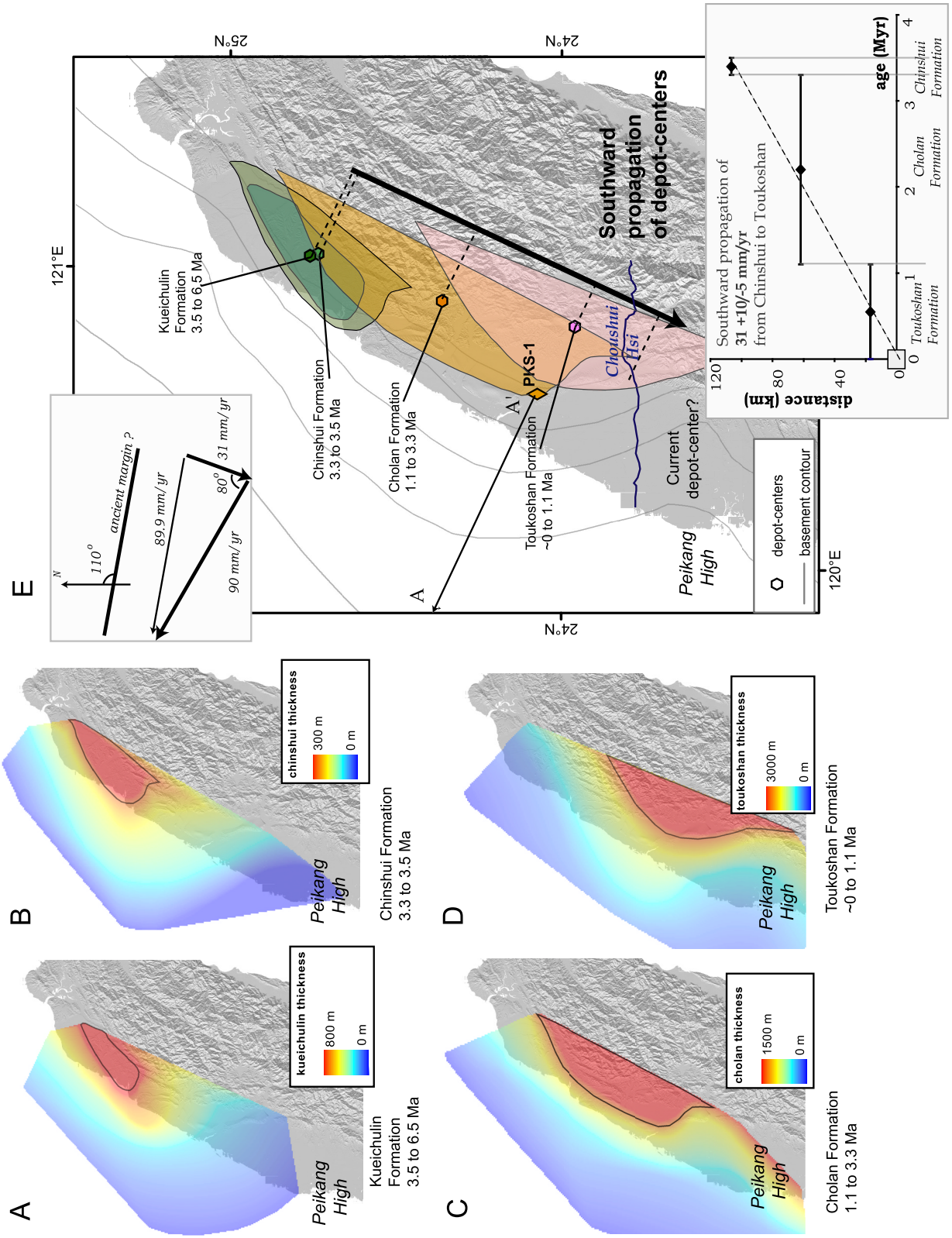
A
Kueichulin Formation
3.5 to 6.5 Ma
Peikang High
kueichulin thickness
800 m
0 m
B
Chinshui Formation
3.3 to 3.5 Ma
chinshui thickness
300 m
0 m
C
Cholan Formation
1.1 to 3.3 Ma
cholan thickness
1500 m
0 m
D
Toukoshan Formation
~0 to 1.1 Ma
toukoshan thickness
3000 m
0 m
E
121°E
120°E
25°N
24°N
Kueichulin Formation 3.5 to 6.5 Ma
Chinshui Formation 3.3 to 3.5 Ma
Cholan Formation 1.1 to 3.3 Ma
Toukoshan Formation ~0 to 1.1 Ma
PKS-1
A
A'
Choushui Hsi
Current depot-center?
Peikang High
Southward propagation of depot-centers
depot-centers
basement contour
N
110°
ancient margin ?
89.9 mm/yr
80°
31 mm/yr
90 mm/yr
Southward propagation of 31 +10/-5 mm/yr from Chinshui to Toukoshan
distance (km)
120
80
40
0
age (Myr)
0
1
2
3
4
Toukoshan Formation
Cholan Formation
Chinshui Formation

Figure 5

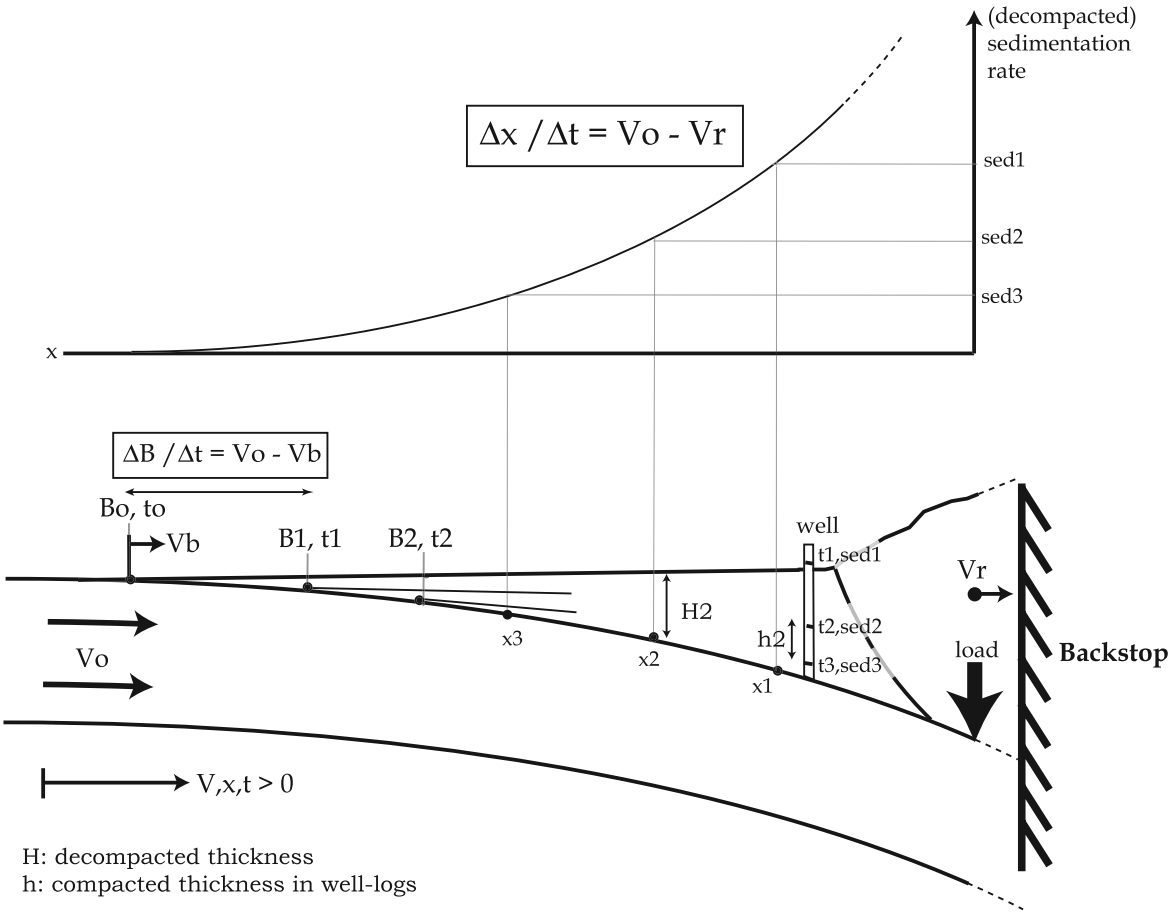

Figure 6. Sketch illustrating how the relative velocity of the footwall toward the load of the range might be retrieved by unrolling sedimentary records. During its migration toward the orogen, a point fixed to the footwall is gradually overlain with sediments. If its sedimentation history is known in a well log record, we might assess the corresponding past positions x_i of the well within the basin provided that the sedimentation pattern is known within the basin. Indeed, in the case of constant sedimentation pattern through time, the decompacted thickness H_i of the sediments lying above the basement can be used to estimate the former position x_i of the point at time t_i within the basin. The load of the range controls the flexure of the footwall and thus the distribution of the sedimentation rates within the foreland. As a result, the retrieved migration is equal to the underthrusting rate $V_o - V_r$, the velocity of the footwall relative to the load of the orogen. This sketch also illustrates the relationship between the past (B_1 and B_2) and present (B_o) positions of the forebulge, and the velocities V_o and V_b in the reference frame defined in Figure 1. Since the sedimentary record of the forebulge (moving at V_b relative to the backstop) is dragged down by the footwall toward the orogen at the velocity V_o, its observed migration over the foreland is equal to the differential rate $V_o - V_b$. In our subsequent analysis of the basin, the origin of the x axis is taken at the present bulge inferred from *Yu and Chou* [2001] and *Lin et al.* [2003].

(Figure 6), and hence $\sim V_o - V_r$ if the geometry of the foreland is assumed to be constrained by the load of the orogenic wedge. The analysis might not be straightforward in the case of Taiwan since the bulge may in fact have been highly unstable because of foreland inelastic yielding [*Chou and Yu*, 2002], so that the hypothesis that $V_r = V_b$ may be a poor approximation [*Waschbusch and Royden*, 1992]. In addition, the various data on the present and past positions of the bulge may not be easily combined together: the past position of the forebulge is estimated for two different epochs (Figure 3) at different latitudes along the range and hence along transects with different temporal evolutions (Figures 3 and 5e). Also, comparison of these past bulges with their present equivalents along the same transects cannot accurately be done since the present bulges inferred by *Lin et al.* [2003] and *Yu and Chou* [2001] are questionable in north central Taiwan.

4.2.2. Migration of the Footwall Relative to the Load of the Range

[14] The spatial distribution of sedimentation rates across the basin is mainly controlled by the flexure related to the orogenic load, which is migrating at a velocity V_r relative to the backstop. Sedimentation rates are highest closer to the orogen, where tectonic subsidence is greater, and taper to zero at the forebulge (Figure 6). The footwall, while converging toward the backstop at a rate V_o keeps a sedimentary record of its position in the basin over time (Figure 6). Such sedimentation history of the footwall can be retrieved through well logs, and

used to assess $V_o - V_r$ (Figures 1 and 6) provided that the sedimentation pattern over the basin is known. To the first order, it might be assumed that this sedimentation pattern compares to the subsidence predicted from the steady state underthrusting of a flexed elastic plate: the idea here is that sedimentation fills the space made available as the foreland is underthrusted beneath the range. In the case of a broken thin plate submitted to a line load at its extremity, the geometry of this plate $w(x')$ follows [*Turcotte and Schubert*, 2002]:

$$w(x') = w_o . \exp\left(-\frac{x'}{\varphi}\right) . \cos\left(\frac{x'}{\varphi}\right) \quad (4)$$

where w_o is the amplitude of the deflection at the location of the line load and φ is the flexural parameter that depends on the flexural rigidity of the plate [*Turcotte and Schubert*, 2002]; x' is the distance away from the line load and equals $D - x$ in the reference frame of Figure 6, where D is the distance between the bulge and the line load. In this case, the pattern of sedimentation sed(x') is governed by the derivative of this curve $w(x')$ with respect to time t:

$$sed(x') = \frac{dw}{dt} = \frac{dw}{dx'} \cdot \frac{dx'}{dt} = (V_o - V_r) \cdot \frac{w_o}{\varphi} \cdot \exp\left(-\frac{x'}{\varphi}\right) \cdot \left[\cos\left(\frac{x'}{\varphi}\right) + \sin\left(\frac{x'}{\varphi}\right)\right] \quad (5)$$

This formulation assumes a constant base level and steady state basin geometry. This theoretical function fits reasonably well the pattern of modern sedimentation rates observed at the mouth of the Choushui Hsi [*Lai and Hsieh*, 2003; *Lee et al.*, 1993]. Given the elastic thickness of ~10 km [*Lin and Watts*, 2002] and the corresponding value for φ, a deflection w at the front of the range of the order of ~2500 m as observed in the Choushui area (Figure 3) yields a rate $V_o - V_r$ of ~50 mm/yr (Figure 7b). In practice, the geometry of the plate might in fact differ from that predicted from this simple equation due to a number of potential complexities. For example, the flexural rigidity might vary along the section, in particular due to inelastic yielding [*Chou and Yu*, 2002] or to lateral geological variations [e.g., *Teng et al.*, 1991]. This equation should not apply, however, to the early stage of development of the basin when the load exerted by the range is increasing with time and when there is no balance between sediment filling and the space made available by the flexure of the underthrusting plate. This is certainly true in our subsequent analysis and in this case a simple logarithmic function was found adequate to fit the isopachs and the well data.

[15] We apply the analysis sketched in Figure 6 to the sedimentation history retrieved from the well PKS-1 (Figure 5) (Simoes et al., submitted manuscript, 2005), which shows an increase in sedimentation rates with time consistent with the eastward migration of the foreland toward the orogen. The well data cover the time of deposition of Toukoshan and upper Cholan formations and thus illustrates the sedimentation history during the filling of the basin in this area of central Taiwan (Figure 5). Since PKS-1 has been incorporated into the range by recent folding of the Pakuashan anticline, we determine its initial location within the foreland by retrodeforming the section based on the fold model and the 1010 m cumulative shortening determined by Simoes et al. (submitted manuscript, 2005). To assess the migrating velocity $V_o - V_r$ of the footwall from this well log, the pattern of sedimentation rate over the basin during the same time period has to be known. To estimate this parameter, the isopachs of the Toukoshan and Cholan formations [*Shaw*, 1996] are decompacted using the same approach as for PKS-1. To avoid underdecompacting or overdecompacting sediments because of the wide depth ranges spanned for each layer, we determine the average porosity and depth by integrating both variables over the depths spanned for each formation. Decompacted thicknesses are then used to estimate average sedimentation rates given the duration of deposition Δt (Table 1). However, the thickness of a vertical section at x has integrated increasing sedimentation rates encountered by the footwall during its translation from $x - (V_o - V_r)\,\Delta t$ to x over the whole time interval Δt (Figure 7a). A correction for this footwall migration over the deposition time Δt is thus needed to retrieve the proper sedimentation rate pattern over the basin: the retrieved pattern is thus dependent on the rate $V_o - V_r$ (Figure 7a). We use a logarithmic function to describe how sedimentation rates vary as a function of distance and adjust the parameters of this function for any given value of $V_o - V_r$ from an iterative scheme.

[16] Different velocities $V_o - V_r$ are tested to retrieve the pattern of sedimentation rates from the Toukoshan and Cholan isopachs and from the sedimentation history of the

Figure 7. Retrieving the long-term sedimentation rate over the foreland basin from sediment thicknesses. (a) Sketch illustrating the analysis performed on the data. The sediment thickness $h[x(t_1)]$ observed presently (t_1) at a certain distance from the backstop within the foreland basin is not representative of the local sedimentation rate at $x(t_1)$. Indeed, this thickness integrates the increasing sedimentation rates that the point, attached to the foreland and presently at $x(t_1)$, went through during its migration toward the orogen since deposition of the sedimentary formation started at t_o. However, this integrative sedimentation rate may be representative of the sedimentation rate at an average position $\bar{x}$ within the foreland. For this analysis, we need to estimate how the sedimentation rate varies as a function of the distance over the basin. (b) Spatial distribution of recent sedimentation and subsidence rates at the mouth of the Choushui Hsi river [*Lai and Hsieh*, 2003; *Lee et al.*, 1993]. The dashed line shows the steady state pattern predicted from the flexure of a thin plate (equation (5)) with an elastic thickness of 10 km [*Lin and Watts*, 2002], flexed at its extremity by a line load located approximately along the LV. This trend shows sedimentation rates lower than the long-term pattern retrieved from $V_o - V_r$ of 45 mm/yr (Figure 8) and approximated here by a logarithmic function (continuous line). Error bars for the data from *Lai and Hsieh* [2003] represent the possible range of values for each site, while those for *Lee et al.*'s [1993] data represent an analytical error of 25%. The origin of the distance axis is taken as the forebulge of *Yu and Chou* [2001] and *Lin et al.* [2003] within the transect A-A′ (Figure 2).

PKS-1 well (Figure 8). These different data sets yield a consistent trend of sedimentation only for $V_o - V_r$ between 45 and 50 mm/yr (Figure 8). In this case, they show a pattern similar to, but with larger values, than that of the modern rates along the transect offshore the mouth of the Choushui further south [*Lee et al.*, 1993] (Figure 7b), which probably represents the current filling of the basin in this region (Figures 3 and 5e). Along the same transect as that of PKS-1, modern sedimentations rates [*Lee et al.*, 1993] are lower than the long-term estimates from Figure 8, by about an order of magnitude. This analysis suggests that the basin filled dominantly during the early stage of basin development, and that the basin in the area of the PKS-1 well has now reached the filled steady state regime.

4.3. Modeling the Spatiotemporal Evolution of the Basin

4.3.1. Development of the Flexural Basin

[17] The geometry of the foreland basin is approximately cylindrical and lines parallel to the mountain belt from north down to the presently subsiding area at the mouth of the Choushui river or even further south (Figures 3 and 5e): this suggests that after the southward migrating high transient sedimentation rates, the basin probably reaches, or at least

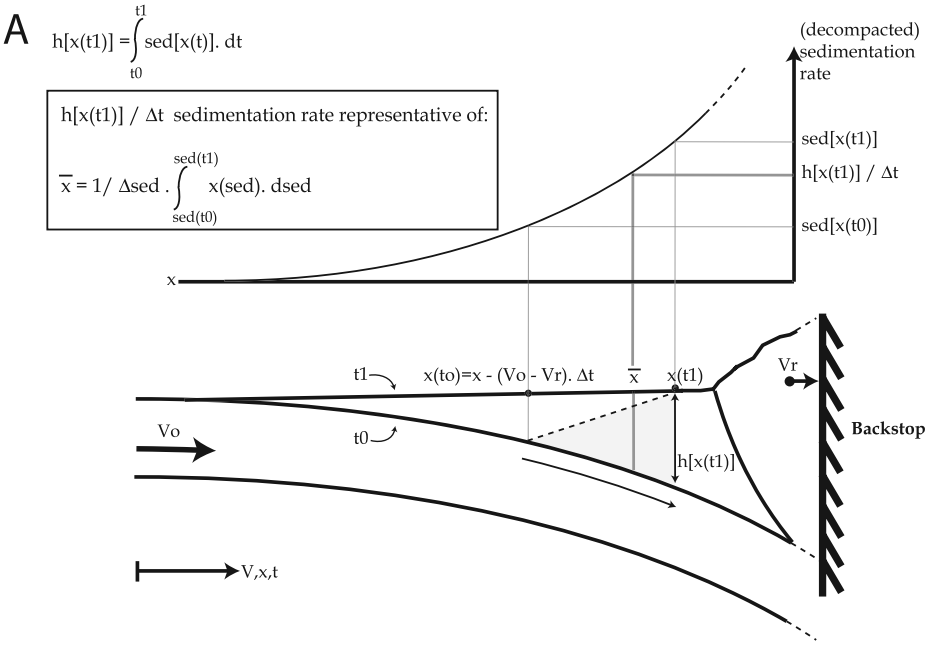

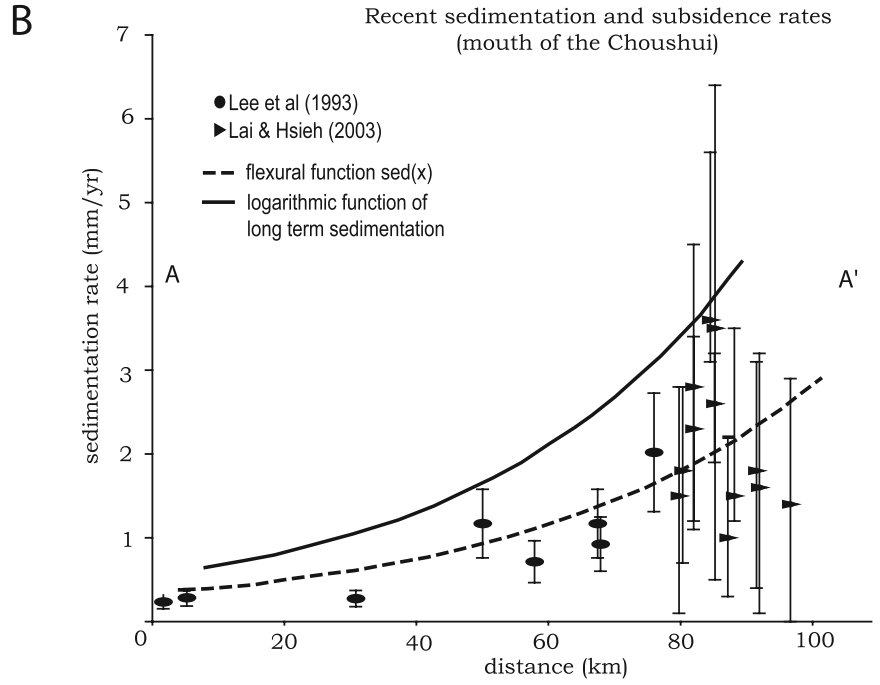

Figure 7

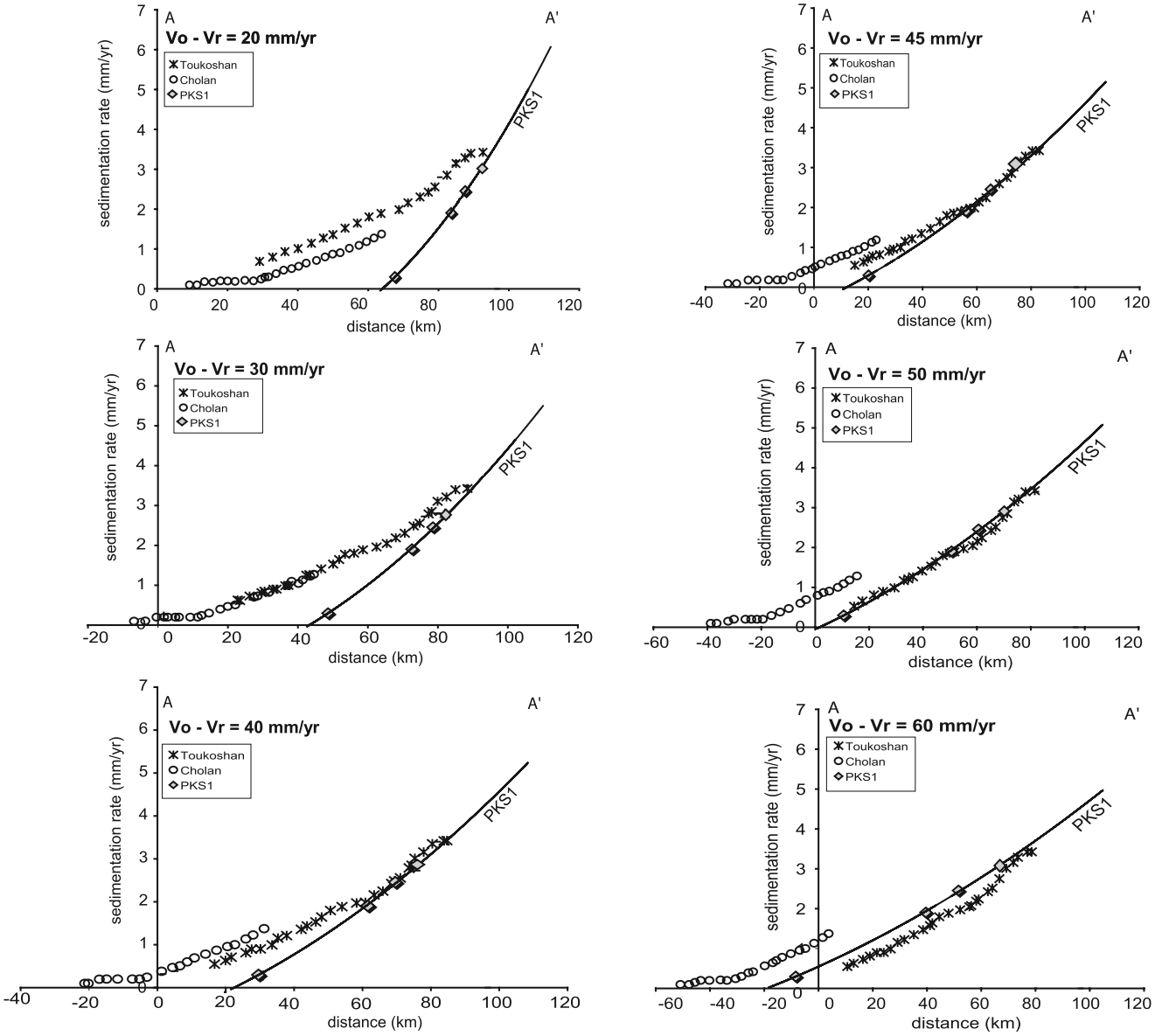

Figure 8. Retrieving $V_o - V_r$ from the sedimentary record of PKS-1 [*Covey*, 1984b; Simoes et al., submitted manuscript, 2005] and the long-term sedimentation rate derived from the sediment thicknesses (Figure 7a). Both the corrected long-term pattern of sedimentation over the foreland (Figure 7) and the translation of time into distance for PKS-1 depend on the assumed rate $V_o - V_r$. Therefore different rates from 20 to 60 mm/yr have been tested. It appears that a good fit between the PKS-1 record and the long-term sedimentation from both Toukoshan and Cholan formations is obtained only for a rate $V_o - V_r$ of 45 to 50 mm/yr. The origin of the distance axis is taken as the forebulge of *Yu and Chou* [2001] and *Lin et al.* [2003] within the transect A-A′ (Figure 2).

approaches, a steady geometry. In addition to that, at the level of the Toukoshan depot center, the decompacted thickness of this formation, and thus the space created to accommodate such amount of sediments, matches the flexed basement (Figure 9), although older synorogenic sediments had also been previously deposited over the footwall (Figures 5a–5c). This indicates that filling of the basin occurs simultaneously with subsidence of the basement under the growing load of the orogen. This contradicts the idea of a time lag between the main episode of flexural subsidence and sediment filling proposed by *Covey* [1986].

4.3.2. Modeling the Southward Propagation of Basin Subsidence and Footwall Migration Toward the Orogen

[18] We consider an initially horizontal line located at sea level representing the undeformed basement, and the long-term sedimentation pattern derived previously (Figure 8) is assumed to represent the subsidence pattern. As it moves at an average rate $V_o - V_r$ of 48 mm/yr toward the load of the range, the basement flexes down. Results for the 2-D modeling of this flexure during the 1.1 Myr long Toukoshan deposition in central Taiwan at the latitude of PKS-1 are illustrated on Figure 9. Each point of the basement has a

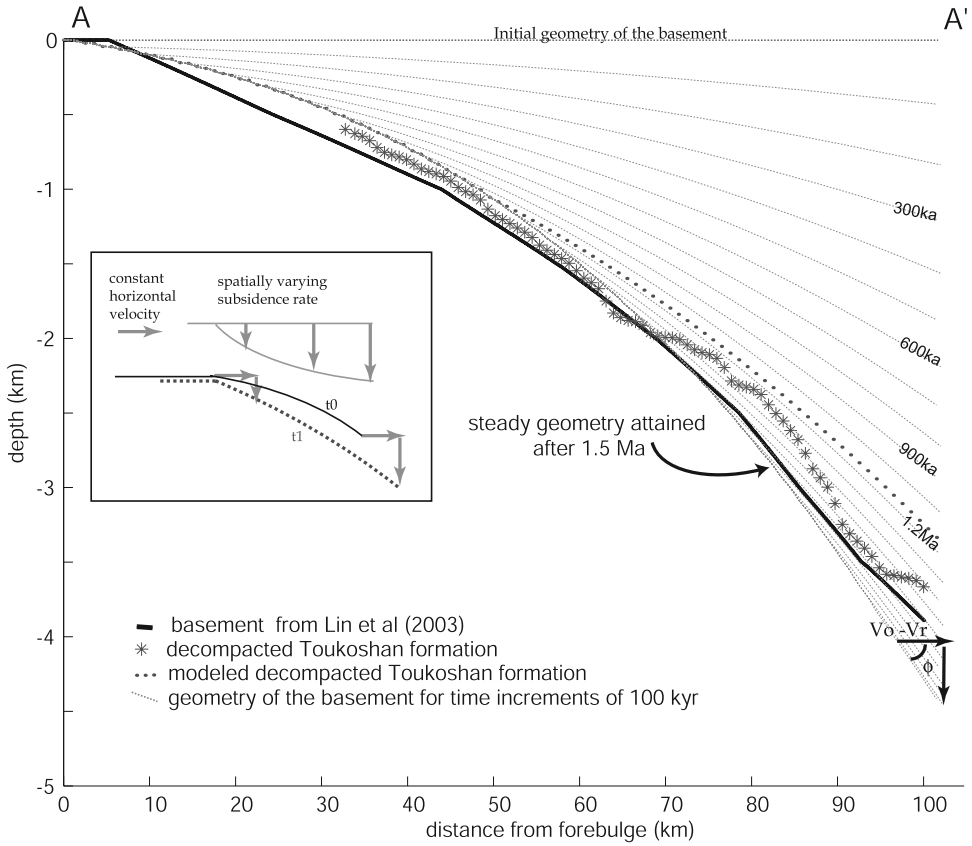

Figure 9. Modeling basin subsidence along transect A-A′ (Figure 2) with the pattern of sedimentation retrieved from the analysis of PKS-1 and the Toukoshan and Cholan formations (Figure 8) and with $V_o - V_r = 48$ mm/yr. The load of the range is here taken as the reference (it is moving at velocity V_r relative to the backstop), and the velocity of each point of the footwall has a horizontal component of 48 mm/yr and a vertical component (subsidence rate) that depends on its position within the foreland basin (inset). The evolution of the predicted geometry of the footwall is shown with time increments of 100 kyr. After 1.1 Ma, the predicted geometry of Toukoshan fits well the observations. In addition to that, the geometry of the basin becomes stationary after ~1.5 Myr.

horizontal velocity $V_o - V_r$ of 48 mm/yr relative to the load of the range, and a subsidence rate commanded by its location within the basin. The subsidence rate is assumed constant over the whole deposition time. Subsidence of the basement occurs very rapidly in the early stages, and evolves toward a steady geometry after ~1.5 Myr, slightly longer than the Toukoshan time period (Figure 9). Such steady state may be attained at each point if the geometry of the basement becomes such that the sedimentation rate is equal to $(V_o - V_r)\tan(\phi)$, where ϕ is the dip angle of the basement (Figure 9). This simple modeling indicates thus that a constant high sedimentation wave probably prevailed offshore central Taiwan during deposition of Toukoshan, for a period of about 1.1 to 1.5 Myr, until the basin reached its present geometry.

[19] Figure 10 shows the results of this modeling extended in three dimensions, where the southward migration of basin subsidence at a rate of 31 mm/yr is integrated. A similar approach is taken as previously, with an initially horizontal surface. The long-term sedimentation pattern as derived from PKS-1 is also assumed (Figure 8). The predicted finite geometry of the basin (Figure 10a) fits relatively well the observed one (Figure 3), although the model fails to predict the lens-shaped geometry of the depot centers (Figures 5a–5d). The lens shapes can be reproduced if it is assumed that high sedimentation rates prevail only for a limited period of time in the early stage of the basin development (Figure 10b). A duration of ~1.5 Myr for the transient high sedimentation rates appears to be indeed needed to obtain depot centers with dimensions similar to those observed (Figure 5). Consequently, this simple geometric model suggests that given the high rates of sedimentation, as well as the fast migration of the foreland toward the orogenic load, it takes ~1.5 Myr for the foreland basin to fill up with sediments and approach or even reach some geometrical steady state. This transient period of early basin filling has recorded the southward propagation of the orogen growth, estimated previously to 31 +10/−5 mm/yr.

5. Kinematics of Deformation Across the Taiwanese Range

5.1. Assessing the Footwall Convergence Velocity V_o

[20] Provided V_r is known, the convergence rate across the orogen V_o can be retrieved from the estimated value of $V_o - V_r$ obtained above. First, we assess the velocity V_f

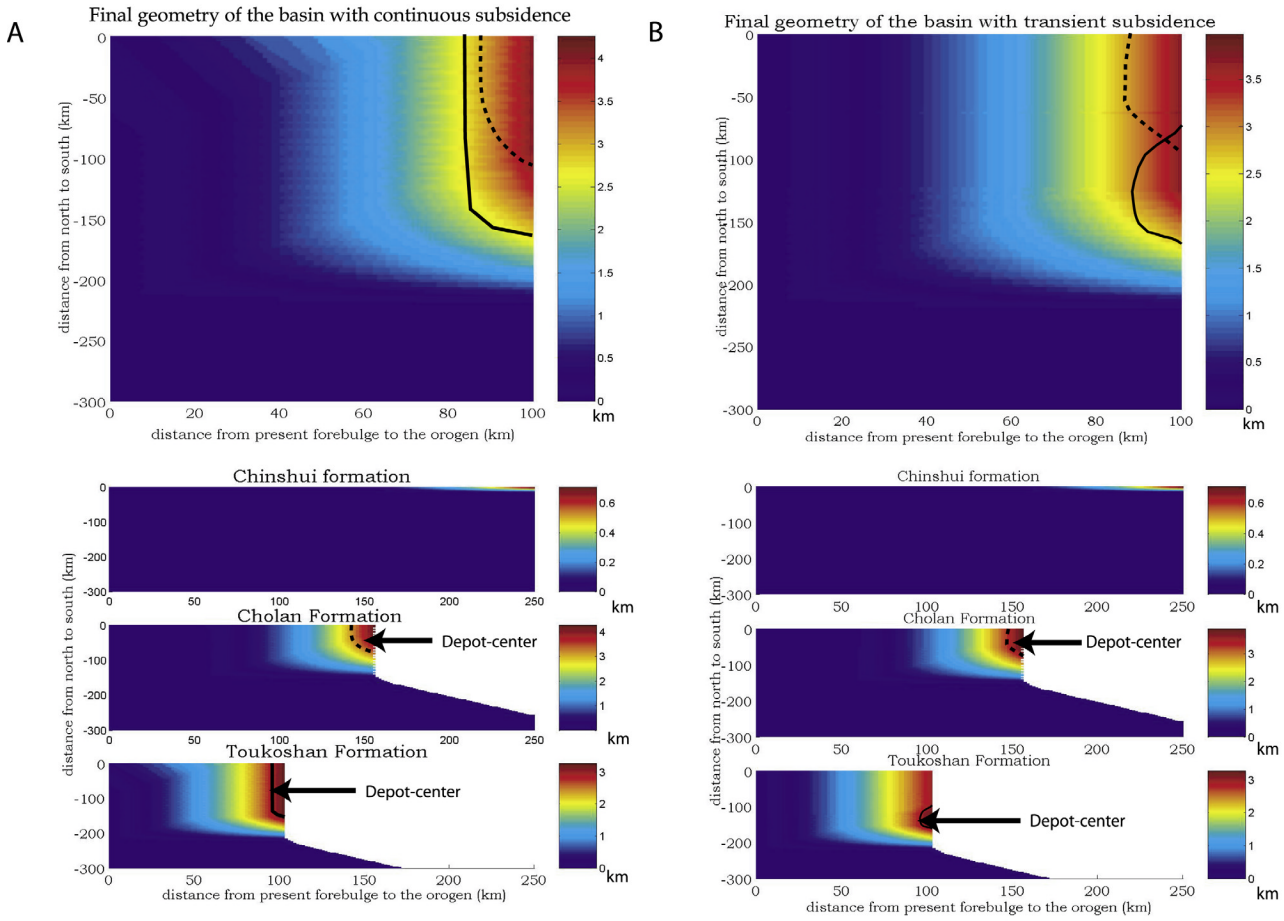

Figure 10. Modeling the foreland basin with account on the 31 mm/yr southward propagation, as well as the 48 mm/yr migration of the foreland toward the load of the orogen (reference here). The predicted final geometry of the basin after 3.5 Myr of development (since the Chinshui Shales) and the modeled decompacted thicknesses of the different formations are illustrated. Color bars represent modeled depth of the basement or else the modeled thickness of decompacted sediments. Depot centers (dashed contours for Cholan formation, solid line for Toukoshan) are defined as the areas within which the modeled sediment thickness exceeds 90% of the maximum predicted value, as for the data shown in Figure 5. Their actual along-strike locations are superposed on the final predicted geometry of the basin by correcting the position of these depot centers from the westward advance of the orogen. This allows only for artificially visualizing their along-strike predicted locations since only the most external portions of the oldest depot centers should be preserved in the basin and may actually be presently observed. (a) In the case of a simple southward migration of the initiation of the high sedimentation derived from our analysis of central Taiwan (Figures 8 and 9). (b) For a 1.5 Myr long transient high-subsidence wave migrating southward and followed by quiescence (see text for further details).

(Figure 1) from the lateral variations of the range width W_r (Figure 2). The northern half of the island has an approximately constant width of ~95 km, while south of the Choushui river, W_r does not exceed ~80 km (Figures 2 and 11). A first-order interpretation is that, during the time period needed for the basin to reach a steady state geometry, which lasts about 1.5 Myr, the range widens by 15 km until it reaches some steady state geometry. An increase of W_r by 15 km in ~1.5 Myr suggests a front migration rate V_f of ~−11 mm/yr. If we now assume that the barycenter of the range load stands approximately halfway between the backstop and the range front (Figure 1), we can estimate V_r to ~−5.5 mm/yr during the same time period. Furthermore, the approximately constant width of ~95 km observed to the north suggests that after this transient widening, V_f and thus V_r tend to ~0. These values of V_f only place an upper bound on the rate V_r. Also, they are highly dependent on how continuous and self-similar the southward evolution of the range is, despite the lateral heterogeneities of the underthrusted margin. These observations imply a long-term convergence V_o across the Taiwan range of ~39.5–44.5 mm/yr.

[21] Underthrusting of basement highs can induce indentation features such as topographic reentrants and conjugate strike-slip faults as commonly observed along subduction zones [e.g., *Dominguez et al.*, 1998a, 1998b; *Lallemand et*

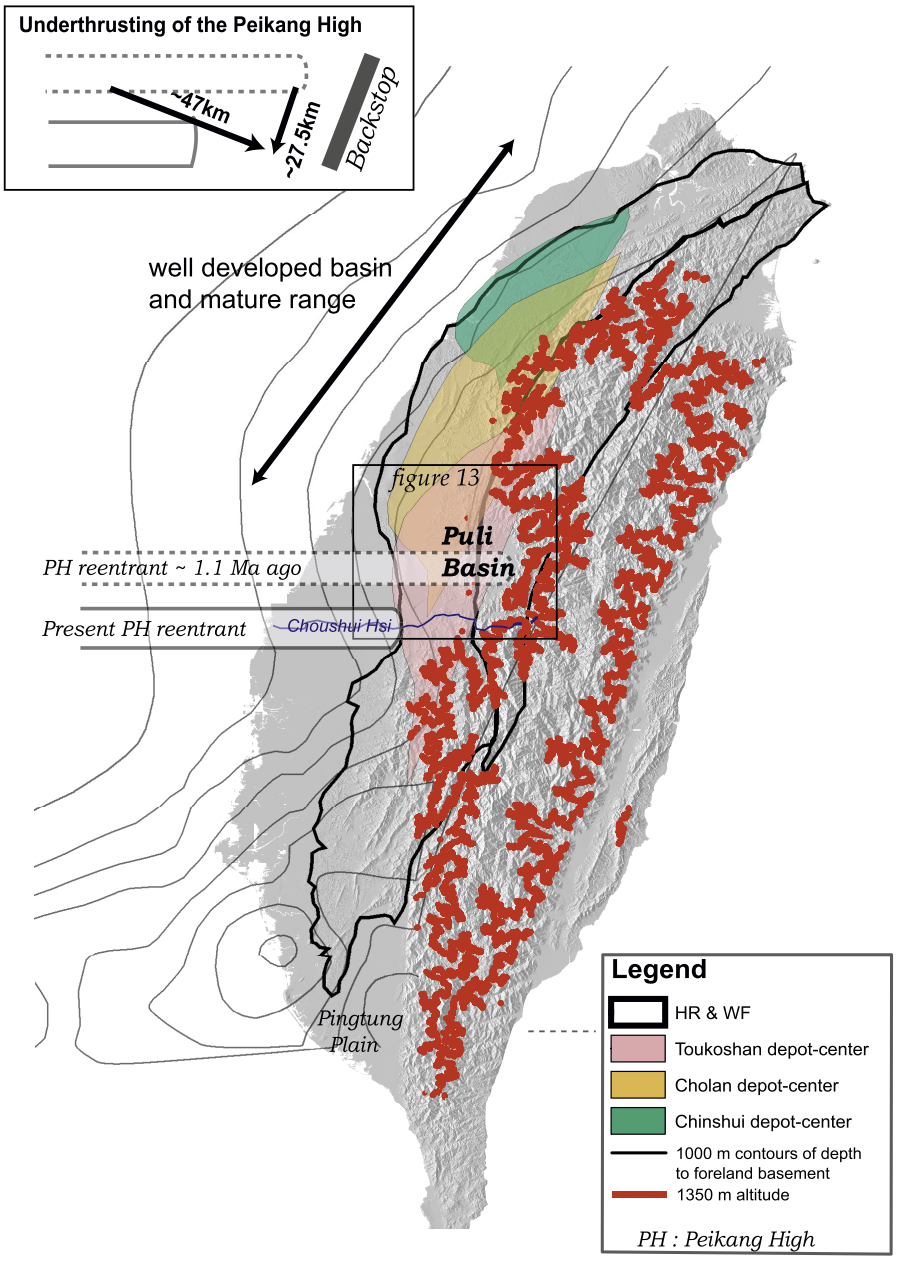

Figure 11. Parallel evolution of the range and basin and kinematics inferred from indentation tectonics of the Peikang High in central Taiwan. Structures of the Taiwan range such as the HR and WF (Figure 2 are reported, as well as the depot centers of the synorogenic formations derived from Figure 5 and the foreland basement depth contours of Figure 3 [*Lin et al.*, 2003]. The 1350 m altitude contour over the range (red line) is shown on the map. Both the present reentrant in the range front related to the indenting Peikang High, as well as its past location as inferred from the arcuate depression of the Puli Basin, are reported. The kinematics that may be inferred by comparing these traces of the underthrusting Peikang High (inset) are consistent with findings from the analysis of the basin and foothills (see text for details).

al., 1992]. The reentrant in the range front observed at the latitude of the Choushui river might be such a feature due to indention by the Peikang High (Figures 2 and 11). This morphological signature is clearly defined, and appears slightly further north than the inferred east-west present position of this margin horst [e.g., *Cheng et al.*, 2003; *Hsu and Sibuet*, 1995; *Lin et al.*, 2003] (Figure 2). Transfer faulting, consistent with indentation tectonics, has been described in the area [*Mouthereau et al.*, 1999]. Keeping the backstop as reference and considering that this structure is attached to the footwall moving at a rate V_o, the point of impact of the Peikang High with the range must have slid progressively southward over time toward its present position. An arcuate geometry similar to the indentation of the present range front is also observed in the topography further northeast around the Puli basin (Figure 11). We

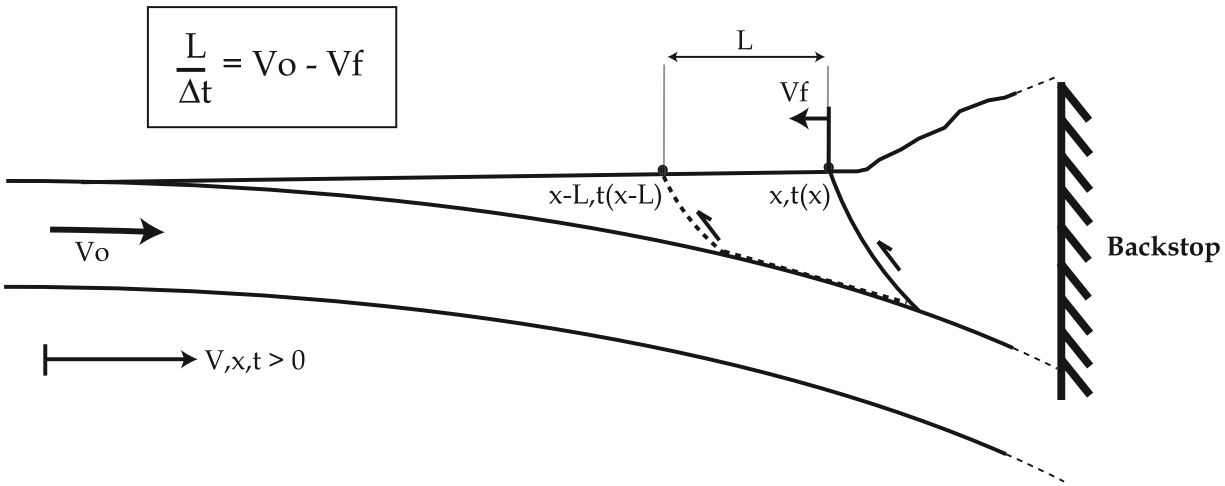

Figure 12. Sketch illustrating how the rate of sediment accretion relates to the velocities defined in Figure 1. Accretion of foreland sediments into the foothills accommodates the relative motion between the footwall and the mountain belt, and more precisely between the foreland and the front of the range. While a slice of sediments with a length L is accreted at time $t(x - L)$, the frontal fault, which also initiated by accretion at time $t(x)$, migrates away from the orogen. However, internal shortening of the new thrust sheet will eventually bring the front back to its initial position relative to the backstop. Therefore, by retrieving the present distance between faults within the WF and by accounting for the finite shortening of the thrust sheets, this accretion rate, which also corresponds to the relative velocity $V_o - V_f$, can be easily assessed.

propose that this morphological depression is also related to the Peikang horst. The Sanyi-Puli strike-slip fault zone [*Chen and Chen*, 2002; *Mouthereau et al.*, 2002] and the alignment of microseismic activity to the south of the Sun-Moon Lake seismic gap embayment [see *Dominguez et al.*, 2003, Figure 2] may reflect also some indentation process. An age of $\sim$ 1.1 Ma may be assigned to this topographic depression: the synorogenic Toukoshan formation, initially deposited in the foreland, is present throughout the whole Puli basin (Figures 5 and 11) and has been subsequently folded. With a rate V_o of 42 mm/yr, the extrapolated position of the Peikang High impact 1.1 Myr ago lies $\sim$47 km to the northeast of the present one, that is precisely immediately west of the Puli depression (Figure 11). This scenario is thus geometrically consistent with our previous estimate of the rate V_o.

5.2. Accretion of Foreland Sediments Within the Foothills

[22] We estimate here the rate of frontal accretion that has resulted from the incorporation into the orogen of the thrust sheets which are now forming the foothills of central Taiwan. These thrust sheets consist of foreland deposits which were scrapped off from the basement. If the age of fault initiation and the initial length of each thrust sheet are known, the rate of sediment accretion $V_o - V_f$ can be derived (Figure 12).

[23] In central Taiwan, this process has resulted from thrusting along three major faults: the Changhua blind thrust, the Chelungpu and Shuangtung faults (Figure 13). The age of initiation of the Changhua blind thrust has been constrained to $\sim$ 65,000 years ago from growth strata in the Pakuashan anticline (Simoes et al., submitted manuscript, 2005) (Figure 13). In the case of the Chelungpu fault, sedimentary and paleomagnetic investigations of the Tsao-huchi section in central Taiwan [*Chen et al.*, 2001] showed no growth features within the Toukoshan deposits older than 0.9 Ma within the hanging wall of the thrust sheet, an observation consistent with the 0.7 Ma age of initiation proposed by *Chen et al.* [2000] based on the analysis of the foreland sedimentation. This same study also proposed on similar arguments that the Shuangtung fault was most probably already active by 1 Ma. Also, since this thrust corresponds to the more internal structure of the WF in the $\sim$1.1 Ma old Puli reentrant, and since it does not show any arcuate geometry related to the passage of the underthrusted Peikang High beneath this area (Figure 13), it certainly dates back to 1.1 Myr ago at most. We thus consider ages of deformation inception of 0.7 Ma and 1.1 Ma for the Chelungpu and Shuangtung faults, respectively (Table 2).

[24] To retrieve the initial lengths of the accreted thrust sheets (L in Figure 12), the present horizontal distances between these major faults in a N110E direction have to be corrected for their cumulated shortening and eventual erosion (Table 2) (Figure 14). The finite shortening on the Changhua thrust has been constrained to 1010 km by Simoes et al. (submitted manuscript, 2005). For the Chelungpu fault, balanced cross sections suggest a minimum shortening of 14 to 16 km [e.g., *Yue et al.*, 2005]. The total shortening on this structure cannot be estimated since the leading edge of the thrust sheet has been eroded by an unknown amount. Altogether, these data suggest a minimum sediment accretion rate $V_0 - V_f$ of $\sim$44 mm/yr over the last 1.1 Myr (Figure 14). This value compares reasonably well with our previous independent estimates of V_o and of the widening rate V_f over the last 1.1 Myr in this region

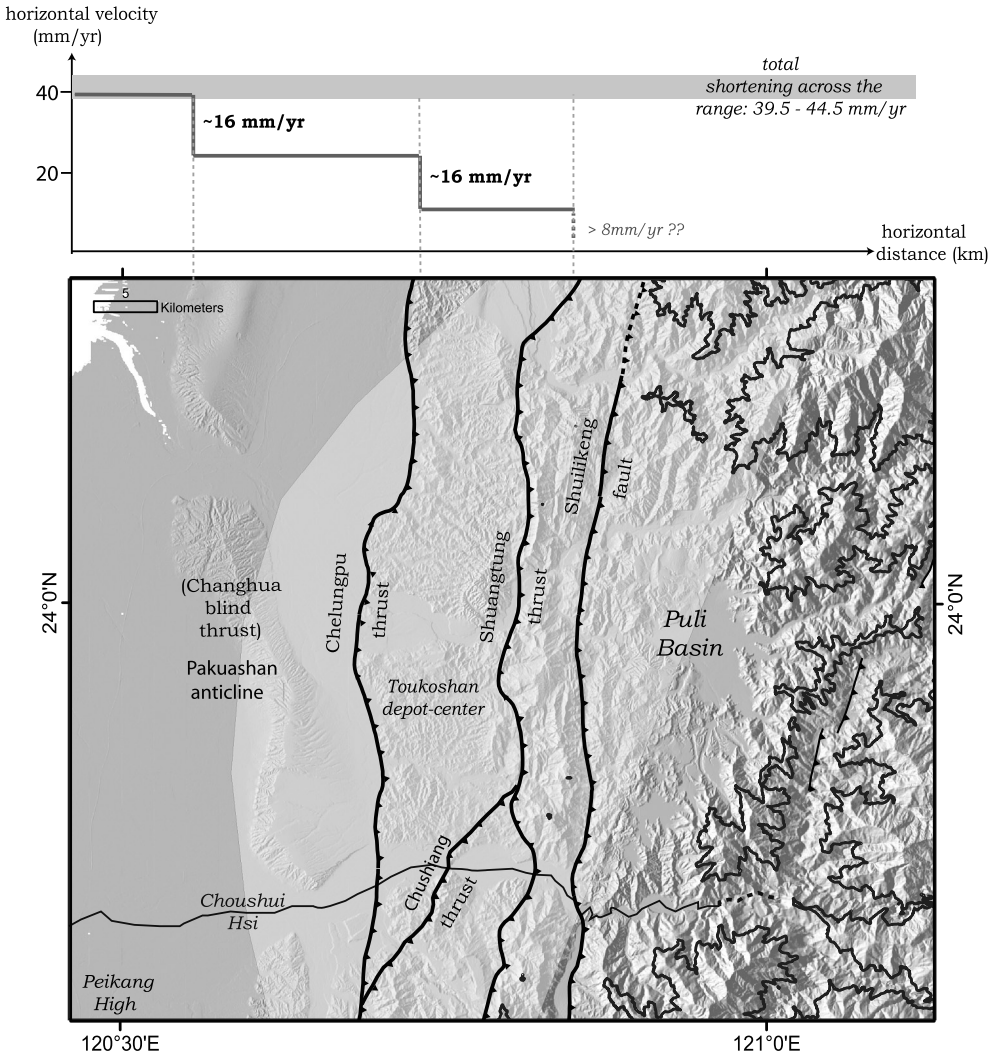

Figure 13. Map of the WF in central Taiwan. The major faults in this area are the Changhua, Chelunpgu, and Shuangtung thrusts from west to east. The Shuilikeng fault, in turn, separates the Foothills from the Hsueshan Range (Figure 2). This fold-and-thrust belt does not show the arcuate geometry of the topography around the Puli depression (Figure 11) and mostly consists of the Toukoshan Formation: it may thus be dated to 1.1 Ma at most. The 1350 m altitude contour line is shown over the topography. Also reported is the long-term horizontal velocity relative to the footwall due to slip on major faults, and how it compares to the proposed total shortening V_o across the range. Rates on the Changhua fault and on the Chelungpu thrust are derived from Simoes et al. (submitted manuscript, 2005) and *Simoes et al.* [2006], respectively. The ~3 mm/yr shortening rate inferred by *Simoes et al.* [2006] on the Chushiang fault is here associated to the Chelungpu fault. The distribution of shortening is given relative to the backstop (Figure 1).

Table 2. Parameters Used to Retrieve the Accretion Rate $V_o - V_f$ for Central Taiwan[a]

Thrust	Distance, km	Shortening, km	L, km	Initiation, years
Changhua	18 ± 2	1.01	19 ± 2	~65,000
Chelungpu	13 ± 1	>14–16	>28 ± 2	~700,000
Shuangtung	13 ± 1	>9?	>28 ± 2	~1,100,000

[a]See Figure 13. The map distances between each thrust have been retrieved north of the Choushui Hsi river to avoid the complexities induced by the underthrusting Peikang High. Finite shortening on the Changhua fault has been documented by Simoes et al. (submitted manuscript, 2005). For the Chelungpu and Shuangtung thrusts, only minimum finite shortening could be retrieved from balanced cross sections of *Yue et al.* [2005]. More particularly, in the case of the Shuangtung thrust, we corrected the 26 km proposed by *Yue et al.* [2005] to 9 km to account for the shortening on the Shuilikeng fault further east. Ages of initiation are retrieved from Simoes et al. (submitted manuscript, 2005), *Chen et al.* [2000], and this study.

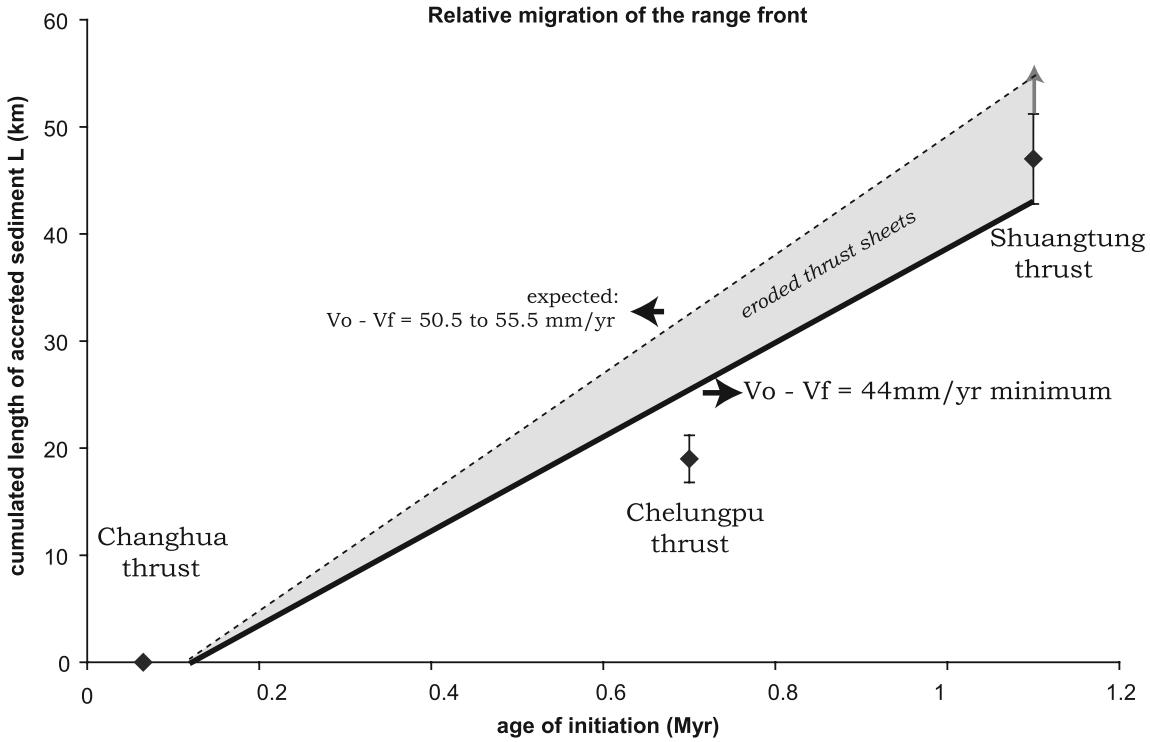

Figure 14. Sediment accretion rate $V_o - V_f$ for central Taiwan (Figure 13). The lengths L of the thrust sheets accreted by each fault, as well as the ages of activity inception are summarized in Table 2. The location of the present frontal thrust, the Changhua blind fault, is taken as the origin to calculate the cumulated values of L. The cumulated length for the Shuangtung is a minimum value since only a lower bound of the total finite shortening on the Chelungpu is known. The accretion rate $V_o - V_f$ of 44 mm/yr is thus a minimum; the difference with the expected 50.5–55.5 mm/yr quantifies horizontal erosion of the thrust sheets.

(Figure 11), which together imply an accretion rate $V_o - V_f$ of 50.5 to 55.5 mm/yr. The 6.5 to 11.5 mm/yr difference between the two values could represent the horizontal erosion of the thrust sheets over this period, in particular here of the Chelungpu thrust sheet. For a fault dip angle of 30°, these horizontal rates would require a vertical erosion rate of 3.7 to 6.6 mm/yr, plausible in light of Holocene river incision rates in the WF [*Dadson et al.*, 2003; Simoes et al., submitted manuscript, 2005]. Given its age of initiation of 0.7 Ma, this implies that ~4.5 to 8.1 km of the initial length of the thrust sheet have been eroded, rising the total finite shortening on the Chelungpu fault to ~18.5 to 24.1 km. No particular constraints may be derived at this point for the Shuangtung thrust sheet.

5.3. Distribution of Shortening Across the Range

[25] The Holocene-Pleistocene shortening rates across the Changhua and Chelungpu thrust faults are estimated to ~16 and ~ up to16 mm/yr, respectively, based on morphotectonic investigations [*Simoes et al.*, 2006, also submitted manuscript, 2005] (Figure 13). These two rates add to a total of ~32 mm/yr, a value close to the 27–45 mm/yr of shortening estimated from geodesy [*Dominguez et al.*, 2003; *Hsu et al.*, 2003; *Loevenbruck et al.*, 2001; *Yu et al.*, 1997]. This suggests that there is currently little internal shortening within the range. The rate on the Changhua fault holds for the last 65,000 years, since it initiated. As for the Chelungpu fault, we have seen that about ~18.5 to 24.1 km of total shortening have been accommodated over the last 0.7 Myr yielding a long-term shortening rate of ~26.4 to 34.4 mm/yr. The presently lower rate on this fault might reflect the recent transfer of horizontal deformation further west to the Changhua fault ~65,000 years ago when it initiated. Indeed, the total ~32 mm/yr presently accommodated on these two most frontal structures definitely compares well with the proposed long-term shortening rate on the Chelungpu fault over 0.7 Myr [*Simoes et al.*, 2006]. Shortening across these two frontal faults is thus taking up most of the total 39.5 to 44.5 mm/yr of shortening across the range. In the case of the more internal faults, the balanced cross section of *Yue et al.* [2005] indicates a minimum finite shortening of 9 km on the Shuangtung thrust when correcting for the Shuilikeng fault. Since 1.1 Ma, this indicates a long-term minimum shortening of ~8.1 mm/yr, sufficient to account for the remaining gap between the ~32 mm/yr on the two most frontal structures and the 39.5–44.5 mm/yr total shortening rate across the range (Figure 13). However, because these rates do not relate to the same period of time, this comparison is only tentative. Since the fold-and-thrust belt of west central Taiwan in the Puli reentrant was emplaced, ~1.1 Myr ago, the range has accommodated a total shortening of about 43.5 to 49 km. Given the total motion on the Changhua (Simoes et al., submitted manuscript, 2005) and on the Chelungpu (with account on

erosion) faults, and by adding the minimum shortening on the Shuangtung thrust of *Yue et al.* [2005], the WF would have taken up a minimum of 28.5 to 34.1 km over the same period. The ~15 km difference between these two estimates could realistically represent erosion of the Shuangtung thrust sheet over this period, and/or eventually some additional shortening on more internal structures such as the Shuilikeng fault (Figure 13). It thus seems that most of the geological shortening across the range over the last 1.1 Myr has been essentially accommodated by the sole active faults of the WF. We thus do not find evidence for any significant cumulative shortening within the more internal portions of the range over this time period.

6. Discussion

6.1. Tectonic Framework of Taiwan and Southward Younging of the Structures

[26] In this section, we discuss how the southward growth of the range may be reflected in the structure of the Central Range (CR) of Taiwan.

[27] Different structural and stratigraphic provinces may be outlined across the CR, west of the LV suture zone [e.g., *Ho*, 1986, 1988] (Figure 2). The most internal and metamorphosed portion of the range is exposed within the Tananao Complex (TC) and is constituted of pre-Tertiary basement [*Faure et al.*, 1991; *Pulver et al.*, 2002]. It is stratigraphically overlain by the metasediments of the slate belt, originally deposited on the passive margin during rifting and opening of the South China Sea [*Ho*, 1986, 1988]. On the basis of their stratigraphy and deformation styles, these metasediments are subdivided into two different provinces [*Clark et al.*, 1993; *Tillman and Byrne*, 1995]: the Backbone Range (BR), and the Hsueshan Range (HR) for which balanced cross sections suggest duplexing structures [*Powell*, 2003]. Over the southern half of Taiwan, the HR narrows and disappears (Figures 2 and 11), so that it may be still buried or simply die out where structures are younger [*Clark et al.*, 1993]. Further west, the WF fold-and-thrust belt has accreted synorogenic sediments of the foreland basin and displays a typical thin-skinned tectonic style [*Suppe*, 1980, 1987]. However, in southern Taiwan, where the WF is widest and the HR fades (Figure 2), structures of the WF appear more complex, with evidence for duplexing of deeper basement rocks within the most internal portions [*Hickman et al.*, 2002; *Hung et al.*, 1999; *Mouthereau et al.*, 2001b; *Suppe*, 1976, 1980], while to the west, thin-skinned tectonics prevail as over central and northern Taiwan [*Hung et al.*, 1999; *Mouthereau et al.*, 2001a]. This architecture of the WF in southern Taiwan strongly resembles the structures observed further north for the HR and WF system, but at a rather less evolved stage. In addition to that, immediately offshore the south WF, the Tainan trough (Figure 2) appears to be filled by ~8–10 km of thick Cenozoic sedimentary sequence [*Lin et al.*, 2003], much alike what is proposed for the HR before its accretion to the CR [*Clark et al.*, 1993; *Lin et al.*, 2003; *Tillman and Byrne*, 1995]. Consequently, we propose to view the most internal portions of the south WF as younger structural equivalents to the HR further north. The region of the Choushui river therefore appears as a structural boundary between the more evolved structures of the HR and WF to the north from their southern structural equivalents (Figures 2 and 11).

6.2. Significance of the Derived Southward Propagation of Orogenic Growth

[28] The spatiotemporal evolution of subsidence in the foreland basin indicates a southward migration of orogen of 31 +10/−5 mm/yr (Figure 5). Errors given for this value essentially reflect the wide time interval covered by deposition of the synorogenic formations. This rate is lower than the rate of ~55 to 90 mm/yr of propagation of the collision derived by assuming that the passive margin and the accreted volcanic arc had geometries similar to those observed presently offshore southern Taiwan [*Byrne and Liu*, 2002; *Suppe*, 1981, 1984]. The discrepancy with our estimate, which is based on the flexural response of the basin to topographic growth, may indicate at face value that the growth of the orogen has propagated southward less rapidly than the collision itself. Another simple alternative is that the actual geometry of the underthrusted margin was not parallel to the one observed further south. The ~90 mm/yr of convergence across the plate boundary predicted by the GPS based global plate model of *Sella et al.* [2002] can be reconciled with a southward propagation of ~31 mm/yr by using the same approach as *Byrne and Liu* [2002] and *Suppe* [1981, 1984] provided that the margin that has entered the collision in north central Taiwan was trending approximately east-west (top inset in Figure 5e). In fact, the Peikang High, which is attributed a roughly east-west trend (Figure 2), marks the southern limit of our investigated area (Figure 5e), and it appears possible that the past margin to the north has had a comparable geometry. However, south of the Choushui river and of this indenting basement horst, the passive margin reveals a more northeast-southwest trend (Figure 2) and it is possible that the ~31 mm/yr rate inferred in this study does not apply for this area. The southward migration rate of collision and of orogenic growth should thus not be taken as laterally continuous, since it highly depends on the structure of the Chinese margin; such idea had actually already been proposed by *Chemenda et al.* [2001]. Also it should be noticed that the ~90 mm/yr convergence rate based on GPS [*Sella et al.*, 2002] may not be representative of the long-term convergence rate across the plate boundary. In any case, the rate proposed in this study is most probably adequate to relate lateral variations and the time evolution of the orogen in central and northern Taiwan. Indeed, the southward migration of the basin development parallels variations in the range width (Figures 2 and 11) and mirrors the evolution of the CR, and in particular of the HR: the presently area where filling of the basin is taking place is located in the region south of the Choushui river and coincides well with the southward fading of the HR into the less evolved structures of the internal south WF. Basin development appears essentially related to the emplacement of the HR, rather than of the CR as a whole (Figures 2 and 11). The TC seems not to contribute significantly to the flexure of the foreland, indicating that the topography may be nearly compensated over this region, probably because of deep processes in the lower crust, or densification of the wedge at depth [e.g., *Goffe et al.*, 2003]. Also, part of the sediments from the TC has been transported to the east rather than

westward, toward the LV basin [e.g., *Chi et al.*, 1981; *Dorsey and Lundberg*, 1988] or the Huatung basin [e.g., *Deschamps et al.*, 1998].

6.3. Shortening Across the Range and Across the Plate Boundary

[29] Plate reconstructions based on magnetic anomalies indicate a long-term convergence of 56 mm/yr of the Philippine Sea Plate relative to Eurasia over the last 15 Myr [*Sibuet et al.*, 2002]. However, such plate reconstructions in this region may be poorly constrained because the Philippine Sea Plate is bounded by active margins. A recent morphotectonic investigation of the LV fault proposed that this structure has taken up ~23 mm/yr over the Holocene [*Shyu et al.*, 2006]. When combined with the ~42 mm/yr shortening rate across the Taiwan range proposed in this study, this rate on the LV fault suggests that the convergence across the plate boundary is presently of at least ~65 mm/yr, which invalidates the rate of 56 mm/yr of *Sibuet et al.* [2002]. Estimates on the total convergence rate across the plate boundary inferred from geodetic measurements relative to the South China block range from ~80 mm/yr [*Seno et al.*, 1993; *Yu et al.*, 1997] to ~90 mm/yr [*Sella et al.*, 2002]. If these rates are also valid over the long term, when compared to the ~65mm/yr taken up across the range on the LV fault, they indicate that ~15 to 25 mm/yr of shortening are to be accommodated further east within the Philippine Sea Plate, elsewhere within the CoR or by the active structures that have been revealed offshore eastern Taiwan [*Malavieille et al.*, 2002]. Better quantifying the contribution of the latter offshore faults to total shortening, as well as assessing whether or not these structures are seismogenic and thus if they can potentially generate earthquakes or tsunamis, is crucial for natural hazards assessment in eastern Taiwan. In any case, estimates of the long-term convergence rate absorbed across the plate boundary, rather than through geodetic measurements, are needed to better constrain how deformation is distributed throughout the whole collision zone.

6.4. Balance Between Incoming and Eroding Fluxes: Evidence for Crustal Subduction

[30] In this section, we assess the balance between incoming and outcoming fluxes for the Taiwan orogen. To derive these fluxes, we use equation (3) and the observed lateral evolution of the range width $W_r(t)$ (Figure 2). We start from a reference at the initial stage $t_o = 0$ to the south of the region considered (Figures 2 and 15). A rate of 31 mm/yr is used to relate lateral variations of the range width to the time evolution of the orogenic wedge, and a shortening rate V_o across the range of 42 mm/yr is assumed. The average long-term erosion rate e can only be approximately estimated. Suspended sediment load measurements over ~30 years in major Taiwanese rivers suggest an average erosion rate of ~3.9 mm/yr, or else 5.5 mm/yr if 30% of bed load is added [*Dadson et al.*, 2003], consistent with the previous results of *Li* [1976] based on similar data. However, such short timescale estimates may be highly variable depending on climatic as well as tectonic events [*Dadson et al.*, 2004]. Over the long term, thermochronology provides the best constraints. However, interpretation and translation of the available data into erosion rates might be highly dependent on the inferred thermal structure. Using a one-dimensional thermal model, *Willett et al.* [2003] estimated erosion rates of 3 to 6 mm/yr over the most internal portion of the CR of Taiwan, which only provides an upper bound value for erosion averaged over the whole range. In our analysis given the uncertainties on this parameter, erosion rate e is varied from 3 to 6 mm/yr. The Moho geometry has been constrained by geophysical studies [*Kim et al.*, 2005; *Lin*, 2005; *Shih et al.*, 1998; *Yeh et al.*, 1998] and its dip angle β has been estimated to ~9–10°E. On the other hand, the dip angle of the basal thrust fault α (Figure 1) is poorly documented. On the basis of relocated microseismicity ($M_L < 3-4$), *Carena et al.* [2002] recently proposed a ~9°E dipping detachment subparallel to the Moho, down to depths of 15 to 16 km over central Taiwan. However, how microseismicity is actually related to structures is still not well understood and there is no guaranty that this estimated geometry also holds for southern Taiwan. Because of all these uncertainties, different values of α (equation (1)) were thus considered in our analysis: 10° after *Carena et al.* [2002] and an arbitrary value of 3°, which we consider to be a lower bound. The average topographic slope, γ, is of ~2–3°. We assume that these parameters do not vary much laterally over the investigated region, which seems reasonable given the homogeneous crustal thickening observed laterally, with Moho depths of ~45 km to the south and ~50 km to the north beneath the easternmost CR [*Lin*, 2005; *Shih et al.*, 1998; *Yeh et al.*, 1998; *Kim et al.*, 2005]. The thickness h of the accreted-underplated slice of footwall into the range is the parameter that will be adjusted in order to fit the observations for any given set of the other parameters (Figure 15). We assume that h is constant along strike and over time.

[31] We first fix e to the minimum value of 3 mm/yr proposed by [*Willett et al.*, 2003] for the CR, and δ to 3°, and vary h. We actually find that the predicted $W_r(t)$ fits well the observations only for a value h of 7 km (Figure 15a). In this case, the northern portion of the Taiwan range has reached the steady state geometry with a width W_r corresponding to W_c = 98 km. Equation (3) predicts a continuous increase in $W_r(t,)$, which is not observed over the southern half of Taiwan and which does not predict the Peikang High reentrant (Figure 15a). Another value for δ of 10°, corresponding to the decollement geometry derived by *Carena et al.* [2002], is tested (Figure 15a). In this case, it appears that the northern portion of the Taiwan range has only approached and not yet reached the steady geometry given by the parameter W_c in equation (3) (here: W_c ~110 km). Other erosion rates up to 6 mm/yr are tested (Figure 15b) and yield different best fitting values of h, up to ~15 km depending on the value considered for δ. Also, Figure 15b indicates that the range to the north of Taiwan would have only reached a stationary geometry if the angle δ is of the order of 3°, and thus if the dip of the basal decollement (α in Figure 1) is of ~17°, which is steeper than proposed by *Carena et al.* [2002] in central Taiwan.

[32] In any case, it seems that only a maximum of 15 km of underthrusted crust can reasonably participate to orogenic growth given the available constraints on erosion (Figure 15b): when compared to the ~28 to 30 km of crust of the Chinese continental margin [*Kim et al.*, 2005; *Lin*,

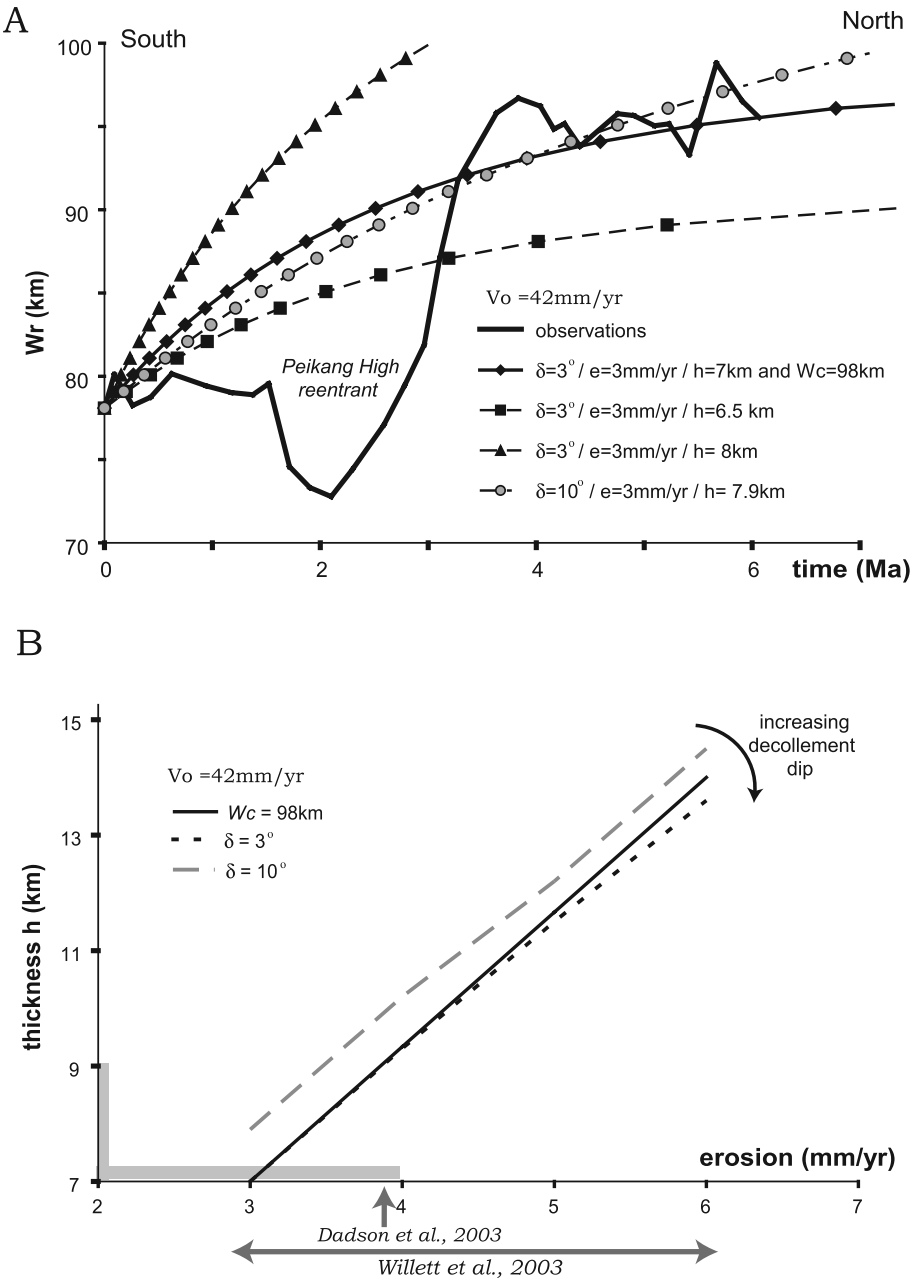

Figure 15. Application of equation (3) to the temporal variation of W_r observed in Taiwan (Figure 2), determined by translating lateral distances into time with the 31 mm/yr southward propagation rate inferred in this study. Initial conditions are taken for the portion of the range immediately north of the Pingtung Plain (Figures 2 and 11), where $W_r(t_o)$ is ~78 km. A shortening rate V_o of 42 mm/yr is considered. (a) Testing different thicknesses h to fit the observed spatiotemporal variation of W_r for different values of δ, and with a long-term average erosion rate e set to 3 mm/yr. Only a small range of values of h for each set of (δ, e) is able to account for the observations. The asymptotic state value W_c is reached faster for lower values of δ. For $\delta = 3°$, the range has attained a steady state geometry to the north (W_c = 98 km) with e = 3 mm/yr and h = 7 km. (b) Thickness of incorporated crust h as a function of the long-term erosion rate e for different values of δ, as needed to fit the observed spatiotemporal variation of W_r shown on Figure 15a. The relation between h and e that is needed in the case that the northern portion of the range has already reached a steady geometry (W_c = 98 km in equation (3)) is also reported (solid line). Long-term values of e over the most internal portions of the range proposed by *Willett et al.* [2003] are shown, as well as the average erosion inferred by *Dadson et al.* [2003] over ~30 years from river suspended load. Highlighted by the gray rectangles are the probable values of h and e as derived from the crustal-scale mass balance (see text for further details).

2005; *Shih et al.*, 1998; *Yeh et al.*, 1998], this implies that crustal subduction must take place in Taiwan (F_{sb} in Figure 1). To fit the overall observed trend in $W_r(t)$ and incorporate into the range the whole underthrusted crust H, the convergence velocity V_o needs to be lowered to ~12 mm/yr, or else average erosion has to be as high as 12 mm/yr: both possibilities can be discarded given the constraints on these parameters. Also, given the geophysical constraints on the Moho geometry beneath the range [*Kim et al.*, 2005; *Lin*, 2005; *Shih et al.*, 1998; *Yeh et al.*, 1998], as well as the geometry of the orogenic prism, we estimate the volume of the crust stored within the wedge and its crustal root to ~2460 km^3 per km of section. If we assume an initial thickness of 30 km [*Shih et al.*, 1998] and 42 mm/yr of shortening, a total volume of 8190 km^3 per km of section has been underthrusted over the last 6.5 Myr. The difference between these two estimates therefore corresponds to the volume of subducted crust: by accounting for the convergence rate and the duration of the collision we obtain from this difference that ~21 km of crust has been subducted into the mantle. This implies that only 7 to 9 km of crust contribute to the growth of the Taiwan orogen and that the long-term erosion rate is therefore of ~2 to 4 mm/yr on average over the whole range (Figure 15b). This crustal-scale mass balance is indeed rather consistent with our previous estimates from the variations of $W_r(t)$. We conclude from these independent reasonings that it is likely that major crustal subduction occurs as argued in a number of previous studies based on different arguments [*Lin*, 1998; *Malavieille et al.*, 2002; *McIntosh et al.*, 2005]. Given the 18 to 22 km thickness of upper crust as imaged by refraction seismics [*Shih et al.*, 1998], our results suggest that only upper crust is incorporated into the range, and that all lower crust is subducted into the mantle. Indeed, no rocks of lower crustal affinity are observed within the orogen. Also, as suggested and reviewed by *McIntosh et al.* [2005], the more mafic probable origin of the lower crust, possibly related to magmatic underplating during the opening of the South China Sea, can facilitate crustal subduction because of lower buoyancy and potential eclogitization during subduction [e.g., *Goffé et al.*, 2003]. It might be surprising though that upper continental crust would also be subducted. However, it has been shown that its density may also increase within the pressure-temperature conditions usually encountered during orogeny [*Bousquet et al.*, 1997; *Goffé et al.*, 2003].

[33] Finally, to better constrain the amount of crust that accounts for the observed orogenic growth, and to further test the crustal-scale mass balance proposed above, more precise estimates on the average erosion rate over the range, as well as better constraints on the geometry of the basal detachment, would be needed. Also, as discussed previously, applying the 31 mm/yr southward propagation rate over southern Taiwan to translate lateral distances into time may not be correct, so that a better estimate of this rate in this region would allow for improving the mass balance after equation (3). A higher migration rate would tend to "squeeze" toward younger ages the observed W_r in southern Taiwan. Last, even though the long-term discrete accretion of rocks may be smoothed by assuming that h is constant over time [*Bollinger et al.*, 2004, Figure 13d], it is possible that this parameter varies along strike, depending for instance on the architecture of the underthrusted margin. However, our previous calculations based on equation (3) are supported by their consistency with the independent estimates derived after the crustal-scale mass balance.

6.5. Testing Previous Models of Mountain Building in Taiwan

[34] The critical wedge theory is one of the most popular models of mountain building, Taiwan being a classical case example [*Barr and Dahlen*, 1989; *Barr et al.*, 1991; *Chapple*, 1978; *Dahlen and Barr*, 1989; *Davis et al.*, 1983]. According to this model the range would maintain a self-similar geometry with a taper angle determined by the friction at the base of the wedge and the internal friction of the wedge material [*Davis et al.*, 1983]. In Taiwan, it has been argued that the range would grow essentially by frontal accretion, and thus by incorporation of thrust sheets at the toe of the wedge [*Barr and Dahlen*, 1989; *Barr et al.*, 1991; *Dahlen and Barr*, 1989]. In this case, shortening is expected to be distributed within the whole range to maintain the amount of thickening of the wedge required to compensate for the loss of material due to erosion [*Avouac*, 2003]. However, our study shows that most of (if not all) the 39.5–44.5 mm/yr of total shortening across the range is rather localized on the frontal faults of the foothills (Figure 13). Such kinematics requires some flux of material into the wedge by underplating in order to compensate for erosion. This kinematics is similar to that proposed for the Himalaya of Nepal where the range is not submitted to any significant internal shortening [*Lave and Avouac*, 2000, 2001], and where underplating beneath the Lesser Himalaya accounts for most of the flux of material into the orogenic wedge [*Bollinger et al.*, 2004, 2006]. This kind of kinematics has been reproduced in sandbox experiments in which horizontal weak zones have been introduced to favor the formation of duplexes within the internal portions of a mountain range [*Konstantinovskaia and Malavieille*, 2005]. In the particular case of Taiwan, such weak zones may be inherited from the complex architecture of the underthrusted margin: this is illustrated by the duplexes beneath the HR [*Powell*, 2003], which has been interpreted as a former half graben of the Chinese margin [*Clark et al.*, 1993; *Lee et al.*, 1997; *Tillman and Byrne*, 1995].

[35] In the particular case of Taiwan, our study indicates that frontal accretion of material is minor. Its contribution to the flux of material incorporated into the range, $(V_o - V_f) \cdot h_f$, can be quantified if h_f, the thickness of material accreted at the front (Figure 1), is known. If this process has been continuous over time, the ~5 km thickness of the thrust sheets observed in the foothills from balanced cross sections could provide an estimate for h_f. Given the maximum value of 15 km previously inferred for h and its most probable estimates of 7 to 9 km (Figure 15b), this would indicate that frontal accretion has contributed to at least a third of the incoming flux of material, a portion too high in light of the kinematics constrained in this study. A possible explanation that reconciles all observations is that thrust sheets have been accreted at the front during discrete events. In this case the observed ~5 km thickness is an upper bound on h_f, averaged over the long term. Such discrete scenario of accretion of material has been also

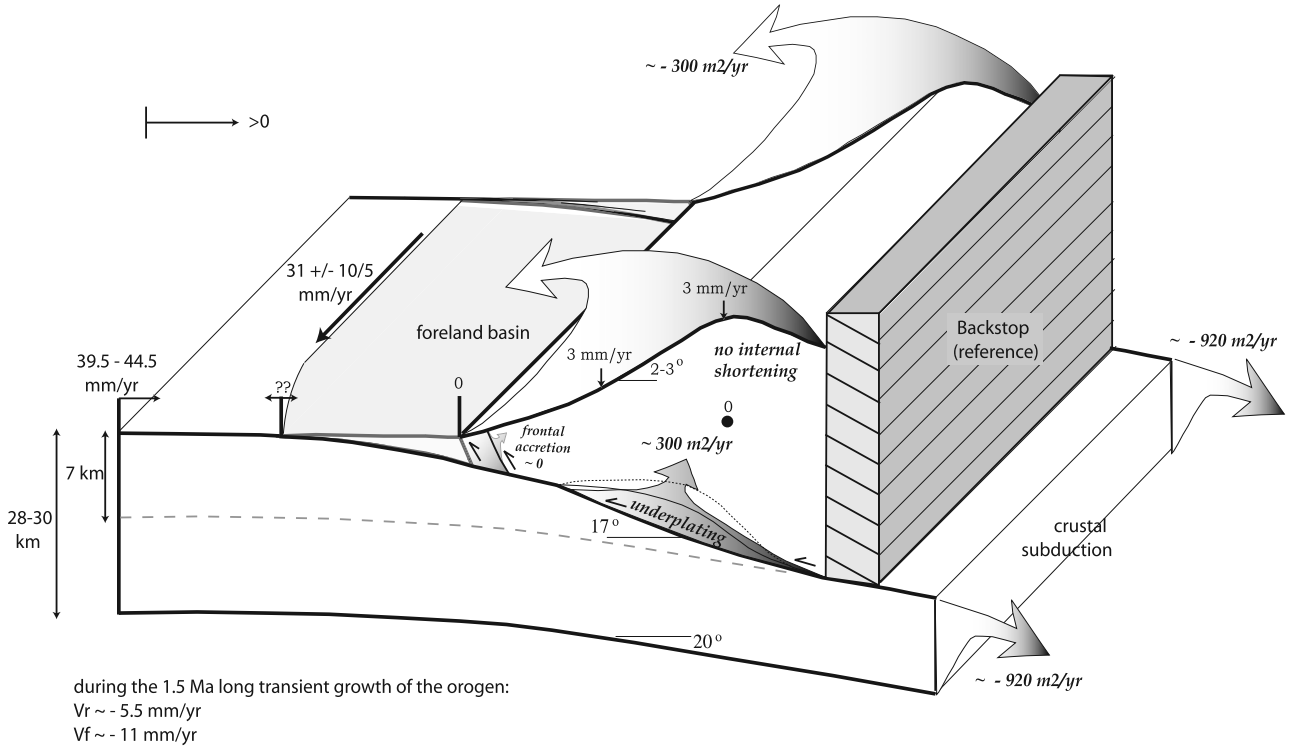

Figure 16. Sketch summarizing the kinematics quantified in this study in the particular case of Taiwan. An average erosion rate of 3 mm/yr has been considered to balance incoming fluxes of material, although this value is not well constrained over the Taiwanese range. In any case it is compatible with an incoming thickness h of ~7 km as deduced from the crustal mass balance, and with a range width W_r of ~98 km as observed in northern Taiwan (Figure 15). The particular case of the range at steady state is illustrated. However, the rates V_f and V_r during the 1.5 Myr long transient maturation of the range are also reported.

proposed for the Lesser Himalaya of Nepal [*Bollinger et al.*, 2004, Figure 13d].

7. Conclusion

[36] Figure 16 summarizes our findings. In Taiwan, the analysis of the spatiotemporal evolution of sedimentation within the foreland basin shows that growth of the orogenic wedge has been propagating to the south by 31 +10/−5 mm/yr. The shortening rate across the range is constrained to 39.5 to 44.5 mm/yr, and appears to be essentially taken up by the most frontal faults of the WF. The flux of crust into the orogen, estimated to be ~300 m^2/yr, has resulted essentially from underplating. A significant fraction of the crust of the underthrusting continental margin is not accreted to the range and is subducted beneath the Philippine Sea plate. Finally, this study places first-order constraints on the kinematics of deformation across the Taiwan orogen that ought to be taken into account in future investigations of the mechanics of mountain building in Taiwan.

[37] **Acknowledgments.** The authors would like to thank Andrew Tien-Shun Lin (NCU, Taiwan) for discussions on the foreland and for providing the data needed for Figure 4, as well as Meng-Long Hsieh (NTU, Taiwan) for his data on the Holocene subsidence rates in the western Coastal Plain. Also, Typhoon Lee (Academia Sinica, Taiwan) and Chen-Feng You (National Cheng-Kung University, Taiwan), as well as Devendra Lal (UCSD, California) and Ala Aldahan (Uppsala University, Sweden) provided helpful insights into the ^{10}Be technique to derive sedimentation rates. Discussions with J. Suppe (University of Princeton) and J. Malavieille (Université Montpellier 2) helped improve the ideas and discussions presented in this manuscript. This paper also benefited from the comments by two anonymous reviewers. This study was partly funded by the Gordon and Betty Moore Foundation. This is Caltech Tectonics Observatory contribution 42.

References

Audet, D. M. (1995), Modelling of porosity evolution and mechanical compaction of calcareous sediments, *Sedimentology*, *42*, 355–373.

Avouac, J. P. (2003), Mountain building, erosion and the seismic cycle in the Nepal Himalaya, in *Adv. Geophys.*, *46*, 1–80, doi:10.1016/S0065-2687(03)46001-9.

Barr, T. D., and F. A. Dahlen (1989), Brittle frictional mountain building: 2. Thermal structure and heat budget, *J. Geophys. Res.*, *94*, 3923–3947.

Barr, T. D., F. A. Dahlen, and D. C. McPhail (1991), Brittle frictional mountain building: 3. Low-grade metamorphism, *J. Geophys. Res.*, *96*, 10,319–10,338.

Beaumont, C. (1981), Foreland basins, *Geophys. J. R. Astron. Soc.*, *65*, 291–329.

Bollinger, L., J. P. Avouac, O. Beyssac, E. J. Catlos, T. M. Harrison, M. Grove, B. Goffe, and S. Sapkota (2004), Thermal structure and exhumation history of the Lesser Himalaya in central Nepal, *Tectonics*, *23*, TC5015, doi:10.1029/2003TC001564.

Bollinger, L., P. Henry, and J. P. Avouac (2006), Mountain building in the Nepal Himalaya: Thermal and kinematic model, *Earth Planet. Sci. Lett.*, *244*, 58–71.

Bousquet, R., B. Goffe, P. Henry, X. Le Pichon, and C. Chopin (1997), Kinematic, thermal and petrological model of the central Alps: Lepontine metamorphism in the upper curst and eclogitisation of the lower crust, *Tectonophysics*, *273*, 105–127.

Byrne, T. B., and C.-S. Liu (2002), Introduction to the geology and geophysics of Taiwan, in *Geology and Geophysics of an Arc-Continent*

Collision, Taiwan, edited by T. B. Byrne and C.-S. Liu, *Spec. Pap. Geol. Soc. Am.*, *358*, V–VIII.

Carena, S., J. Suppe, and H. Kao (2002), Active detachment of Taiwan illuminated by small earthquakes and its control of first-order topography, *Geology*, *30*, 935–938.

Chang, S. S. L., and W. R. Chi (1983), Neogene nannoplankton biostratigraphy in Taiwan and the tectonic implications, *Pet. Geol. Taiwan.*, *19*, 93–147.

Chapple, W. M. (1978), Mechanics of thin-skinned fold-and-thrust belts, *Geol. Soc. Am. Bull.*, *89*, 1189–1198.

Chemenda, A. I., R.-K. Yang, J.-F. Stephan, E. A. Konstantinovskaya, and G. M. Ivanov (2001), New results from physical modelling of arc-continent collision on Taiwan: Evolutionary model, *Tectonophysics*, *333*, 159–178.

Chen, C. C., and C.-S. Chen (2002), Sanyi-Puli conductivity anomaly in NW Taiwan and its implication for the tectonics of the 1999 Chi-Chi earthquake, *Geophys. Res. Lett.*, *29*(8), 1166, doi:10.1029/2001GL013890.

Chen, W.-S., et al. (2000), The evolution of foreland basins in the western Taiwan: Evidence from the Plio-Pleistocene sequences, *Bull. Cent. Geol. Surv.*, *13*, 136–156.

Chen, W.-S., K. D. Ridgway, C.-S. Horng, Y.-G. Chen, K.-S. Shea, and M.-G. Yeh (2001), Stratigraphic architecture, magnetostratigraphy, and incised-valley systems of the Pliocene-Pleistocene collisional marine foreland basin of Taiwan, *Geol. Soc. Am. Bull.*, *113*, 1249–1271.

Cheng, W. B., H.-C. Huang, C. Wang, M.-S. Wu, and T.-H. Hsiuan (2003), Velocity structure, seismicity, and fault structure in the Peikang High area of Western Taiwan, *Terr. Atmos. Oceanic Sci.*, *14*, 63–83.

Chi, W. R., and H.-M. Huang (1981), Nannobiostratigraphy and paleoenvironments of the late Neogene sediments and their tectonic implications in the Miaoli area, Taiwan, *Pet. Geol. Taiwan*, *18*, 111–129.

Chi, W. R., J. Namson, and J. Suppe (1981), Stratigraphic record of plate interactions in the coastal range of eastern Taiwan, *Mem. Geol. Soc. China.*, *4*, 155–194.

Chou, Y.-W., and H.-S. Yu (2002), Structural expressions of flexural extension in the arc-continent collisional foredeep of western Taiwan, in *Geology and Geophysics of an Arc-Continent Collision*, edited by T. B. Byrne and C.-S. Liu, *Spec. Pap. Geol. Soc. Am.*, *358*, 1–12.

Clark, M. B., D. M. Fisher, C.-Y. Lu, and C.-H. Chen (1993), Kinematic analyses of the Hsueshan range, Taiwan: A large-scale pop-up structure, *Tectonics*, *12*, 205–217.

Covey, M. (1984a), Lithofacies analysis and basin reconstruction, Plio-Pleistocene western Taiwan foredeep, *Pet. Geol. Taiwan*, *20*, 53–83.

Covey, M. (1984b), Sedimentary and tectonic evolution of the western Taiwan foredeep, Ph.D. thesis, 152 pp., Princeton Univ., Princeton, N. J.

Covey, M. (1986), The evolution of foreland basins to steady-state: Evidence from the western Taiwan foreland basin, *Spec. Publ. Int. Assoc. Sedimentol.*, *8*, 77–90.

Dadson, S. J., et al. (2003), Links between erosion, runoff variability and seismicity in the Taiwan orogen, *Nature*, *426*, 648–651.

Dadson, S. J., et al. (2004), Earthquake-triggered increase in sediment delivery from an active mountain belt, *Geology*, *32*, 733–736.

Dahlen, F. A., and T. D. Barr (1989), Brittle frictional mountain building: 1. Deformation and mechanical energy budget, *J. Geophys. Res.*, *94*, 3906–3922.

Davis, D., J. Suppe, and F. A. Dahlen (1983), Mechanics of fold-and-thrust belts and accretionary wedges, *J. Geophys. Res.*, *88*, 1153–1172.

DeCelles, P. G., and P. C. DeCelles (2001), Rates of shortening, propagation, underthrusting, and flexural wave migration in continental orogenic systems, *Geology*, *29*, 135–138.

Deschamps, A., S. Lallemand, and J.-Y. Collot (1998), A detailed study of the Gagua Ridge: A fracture zone uplifted during a plate reorganisation in the mid-Eocene, *Mar. Geophys. Res.*, *20*, 403–423.

Dominguez, S., S. Lallemand, J. Malavieille, and P. Schnurle (1998a), Oblique subduction of the Gagua Ridge beneath the Ryukyu accretionary wedge system: Insights from marine observations and sandbox experiments, *Mar. Geophys. Res.*, *20*, 383–402.

Dominguez, S., S. Lallemand, J. Malavieille, and R. von Huene (1998b), Upper plate deformation associated with seamount subduction, *Tectonophysics*, *293*, 207–224.

Dominguez, S., J. P. Avouac, and M. Remi (2003), Horizontal coseismic deformation of the 1999 Chi-Chi earthquake measured from SPOT satellite images: Implications for the seismic cycle along the western foothills of central Taiwan, *J. Geophys. Res.*, *108*(B2), 2083, doi:10.1029/2001JB000951.

Dorsey, R. J., and N. Lundberg (1988), Lithofacies analysis and basin reconstruction of the Plio-Pleistocene collisional basin, Coastal Range of eastern Taiwan, *Acta Geol. Taiwan.*, *26*, 57–132.

Faure, M., C. Y. Lu, and H. T. Chu (1991), Ductile deformation and Miocene nappe-stacking in Taiwan related to motion of the Philippine Sea Plate, *Tectonophysics*, *198*, 95–105.

Goffe, B., R. Bousquet, P. Henry, and X. Le Pichon (2003), Effect of the chemical composition of the crust on the metamorphic evolution of orogenic wedges, *J. Metamorph. Geol.*, *21*, 123–141.

Hetland, E. A., and F. T. Wu (1998), Deformation of the Philippine Sea Plate under the coastal range, Taiwan: Results from an offshore-onshore seismic experiment, *Terr. Atmos. Ocean. Sci.*, *9*, 363–378.

Hickman, J. B., D. V. Wiltschko, J.-H. Hung, P. Fang, and Y. Bock (2002), Structure and evolution of the active fold-and-thrust belt of southwestern Taiwan from Global Positioning System analysis, in *Geology and Geophysics of an Arc-Continent Collision*, edited by T. B. Byrne and C.-S. Liu, *Spec. Pap. Geol. Soc. Am.*, *358*, 75–92.

Ho, C. S. (1986), A synthesis of the geologic evolution of Taiwan, *Tectonophysics*, *125*, 1–16.

Ho, C. S. (1988), *An Introduction to the Geology of Taiwan:- Explanatory Text of the Geologic Map of Taiwan*, 2nd ed., 192 pp., Cent. Geol. Surv., Taipei, Taiwan.

Horng, C.-S., and K.-S. Shea (1996), Dating of the Plio-Pleistocene rapidly deposited sequence based on integrated magneto-biostratigraphy: A case study of the Magida-Chi section, Coastal Range, eastern Taiwan, *J. Geol. Soc. China.*, *39*, 31–58.

Hsu, S. K., and J. C. Sibuet (1995), Is Taiwan the result of arc-continent or arc-arc collision?, *Earth Planet. Sci. Lett.*, *136*, 315–324.

Hsu, Y.-J., M. Simons, S.-B. Yu, L.-C. Kuo, and H.-Y. Chen (2003), A two-dimensional dislocation model for interseismic deformation of the Taiwan mountain belt, *Earth Planet. Sci. Lett.*, *211*, 287–294.

Huang, T. (1984), Planktic foraminiferal biostratigraphy and datum planes in the Neogene sedimentary sequence in Taiwan, *Paleogeogeogr. Paleoclimatol. Paleoecol.*, *46*, 97–106.

Hung, J.-H., D. V. Wiltschko, H.-C. Lin, J. B. Hickman, P. Fang, and Y. Bock (1999), Structure and motion of the southwestern Taiwan fold and thrust belt, *Terr. Atmos. Oceanic Sci.*, *10*, 543–568.

Jordan, T. E. (1981), Thrust loads and foreland basin evolution, Cretaceous, western United States, *AAPG Bull.*, *65*, 2506–2520.

Kim, K.-H., J.-M. Chiu, J. Pujol, K. C. Chen, B. S. Huang, Y. H. Yeh, and P. Shen (2005), Three-dimensional Vp and Vs structural models associated with the active subduction and collision tectonics in the Taiwan region, *Geophys. J. Int.*, *162*, 204–220.

Konstantinovskaia, E., and J. Malavieille (2005), Erosion and exhumation in accretionary orogens: Experimental and geological approaches, *Geochem. Geophys. Geosyst.*, *6*, Q02006, doi:10.1029/2004GC000794.

Lai, T.-H., and M.-L. Hsieh (2003), Late-Quaternary vertical rock-movement rates of the coastal plains of Taiwan, paper presented at Geological Society of Taiwan Meeting, Taipei.

Lallemand, S., J. Malavieille, and S. Calassou (1992), Effects of oceanic ridge subduction on accretionary wedges: Experimental modeling and marine observations, *Tectonics*, *11*, 1301–1313.

Lave, J., and J. P. Avouac (2000), Active folding of fluvial terraces across the Siwaliks Hills, Himalayas of central Nepal, *J. Geophys. Res.*, *105*, 5735–5770.

Lave, J., and J. P. Avouac (2001), Fluvial incision and tectonic uplift across the Himalayas of central Nepal, *J. Geophys. Res.*, *106*, 26,561–26,591.

Lee, J.-C., J. Angelier, and H. T. Chu (1997), Polyphase history and kinematics of a complex major fault zone in the northern Taiwan mountain belt: The Lishan fault, *Tectonophysics*, *274*, 97–115.

Lee, T., C.-F. You, and T.-K. Liu (1993), Model-dependent 10Be sedimentation rate for the Taiwan Strait and their tectonic significance, *Geology*, *21*, 423–426.

Li, Y.-H. (1976), Denudation of Taiwan island since the Pliocene epoch, *Geology*, *4*, 105–107.

Lin, A. T., and A. B. Watts (2002), Origin of the west Taiwan basin by orogenic loading and flexure of a rifted continental margin, *J. Geophys. Res.*, *107*(B9), 2185, doi:10.1029/2001JB000669.

Lin, A. T., A. B. Watts, and S. P. Hesselbo (2003), Cenozoic stratigraphy and subsidence history of the South China Sea margin in the Taiwan region, *Basin Res.*, *15*, 453–478.

Lin, C. H. (1998), Tectonic implications of an aseismic belt beneath Eastern Central range of Taiwan: Crustal subduction and exhumation, *J. Geol. Soc. China*, *41*, 441–460.

Lin, C. H. (2005), Identification of mantle reflections from a dense linear seismic array: Tectonic implications to the Taiwan orogeny, *Geophys. Res. Lett.*, *32*, L06315, doi:10.1029/2004GL021814.

Liu, T.-K., S. Hsieh, Y.-G. Chen, and W.-S. Chen (2001), Thermo-kinematic evolution of the Taiwan oblique-collision mountain belt as revealed by zircon fission-track dating, *Earth Planet. Sci. Lett.*, *186*, 45–56.

Loevenbruck, A., R. Cattin, X. Le Pichon, M.-L. Courty, and S.-B. Yu (2001), Seismic cycle in Taiwan derived from GPS measurements, *C. R. Acad. Sci.*, *333*, 57–64.

Lyon-Caen, H., and P. Molnar (1985), Gravity anomalies, flexure of the Indian plate, and the structure, support and evolution of the Himalaya and Ganga Basin, *Tectonics*, *4*, 513–538.

Malavieille, J., S. E. Lallemand, S. Dominguez, A. Deschamps, C.-Y. Lu, C.-S. Liu, P. Schnurle, and A. S. Crew (2002), Arc-continent collision in Taiwan: New marine observations and tectonic evolution, in *Geology and Geophysics of an Arc-Continent Collision*, edited by T. B. Byrne and C.-S. Liu, *Spec. Pap. Geol. Soc. Am.*, *358*, 189–213.

McIntosh, K., Y. Nakamura, T.-K. Wang, R. C. Shih, A. Chen, and C. S. Liu (2005), Crustal-scale seismic profiles across Taiwan and the Western Philippine Sea, *Tectonophysics*, *401*, 23–54.

Mouthereau, F., O. Lacombe, B. Deffontaines, J. Angelier, and H. T. Chu (1999), Quaternary transfer faulting and belt front deformation at Pakuashan (western Taiwan), *Tectonics*, *18*, 215–230.

Mouthereau, F., J. Angelier, and J. C. Lee (2001a), The 21-September-1999 earthquake: Structural inheritance and basement involvement at the front of the Taiwan mountain, *C. R. Acad. Sci., Ser. IIA*, *333*, 93–103.

Mouthereau, F., O. Lacombe, B. Deffontaines, J. Angelier, and S. Brusset (2001b), Deformation history of the southwestern Taiwan foreland thrust belt: Insights from tectono-sedimentary analyses and balanced cross-sections, *Tectonophysics*, *333*, 293–322.

Mouthereau, F., B. Deffontaines, O. Lacombe, and J. Angelier (2002), Variations along the strike of the Taiwan thrust belt: Basement control on structural style, wedge geometry, and kinematics, in *Geology and Geophysics of an Arc-Continent Collision, Taiwan*, edited by T. B. Byrne and C.-S. Liu, in *Geology and Geophysics of an Arc-Continent Collision*, edited by T. B. Byrne and C.-S. Liu, *Spec. Pap. Geol. Soc. Am.*, *358*, 35–58.

Powell, L. K. (2003), Feedback between erosion and fault reactivation in the Puli Basin: Hsueshan belt of central Taiwan, Master thesis, 61 pp, Univ. of Colorado, Boulder.

Pulver, M. H., J. M. Crespi, and T. B. Byrne (2002), Lateral extrusion in a transpressional collision zone: An example from the pre-Tertiary metamorphic basement of Taiwan, in *Geology and Geophysics of an Arc-Continent Collision, Taiwan*, edited by T. B. Byrne and C. S. Liu, *Spec. Pap. Geol. Soc. of Am.*, *358*, 107–120.

Sella, G. F., T. H. Dixon, and A. Mao (2002), REVEL: A model for recent plate velocities from space geodesy, *J. Geophys. Res.*, *107*(B4), 2081, doi:10.1029/2000JB000033.

Seno, T., S. Stein, and A. E. Gripp (1993), A model for the motion of the Philippine Sea plate consistent with NUVEL-1 and geological data, *J. Geophys. Res.*, *98*, 17,941–17,948.

Shaw, C. L. (1996), Stratigraphic correlation and isopach maps of the western Taiwan Basin, *Terr. Atmos. Oceanic Sci.*, *7*, 333–660.

Shih, R. C., C. H. Lin, H. L. Lai, Y. H. Yeh, B. S. Huang, and H. Y. Yen (1998), Preliminary crustal structures across Central Taiwan from modeling of the onshore/offshore wide-angle seismic data, *Terr. Atmos. Oceanic Sci.*, *9*, 317–328.

Shyu, J. B. H., K. Sieh, and Y.-G. Chen (2005), Neotectonic architecture of Taiwan and its implications for future large earthquakes, *J. Geophys. Res.*, *110*, B08402, doi:10.1029/2004JB003251.

Shyu, J. B. H., K. Sieh, J. P. Avouac, W.-S. Chen, and Y.-G. Chen (2006), Millenial slip rate of the Longitudinal Valley fault from river terraces: Implications for convergence across the active suture of eastern Taiwan, *J. Geophys. Res.*, *111*, B08403, doi:10.1029/2005JB003971.

Sibuet, J. C., S. K. Hsu, X. Le Pichon, J.-P. Le Formal, D. Reed, G. Moore, and C. S. Liu (2002), East-Asia plate tectonics since 15 Ma: Constraints from the Taiwan region, *Tectonophysics*, *344*, 103–134.

Simoes, M., J. P. Avouac, and Y.-G. Chen (2006), Slip rates on the Chelungpu and Chushiang thrust faults, inferred from a deformed strath terrace along the Dungpuna river, west central Taiwan, *J. Geophys. Res.*, doi:10.1029/2005JB004200, in press.

Suppe, J. (1976), Decollement folding in southwestern Taiwan, *Pet. Geol. Taiwan.*, *13*, 26–35.

Suppe, J. (1980), Imbricated structure of Western Foothills Belt, south central Taiwan, *Pet. Geol. Taiwan.*, *17*, 1–16.

Suppe, J. (1981), Mechanics of mountain building and metamorphism in Taiwan, *Mem. Geol. Soc. China*, *4*, 67–89.

Suppe, J. (1984), Kinematics of arc-continent collision, flipping of subduction, and back-arc spreading near Taiwan, *Mem. Geol. Soc. China*, *6*, 21–33.

Suppe, J. (1987), The active Taiwan mountain belt, in *The Anatomy of Mountain Ranges*, edited by J.-P. Schaer and J. Rodgers, pp. 277–293, Princeton Univ. Press, Princeton, N. J.

Teng, L. S. (1987), Stratigraphic records of the late Cenozoic Penglai orogeny of Taiwan, *Acta Geol. Taiwan.*, *25*, 205–224.

Teng, L. S., Y. Wang, C.-H. Tang, C. Y. Huang, T.-C. Huang, M.-S. Yu, and A. Ke (1991), Tectonic aspects of the Paleogene depositional basin of northern Taiwan, *Proc. Geol. Soc. China*, *34*, 313–336.

Tillman, K. S., and T. B. Byrne (1995), Kinematic analysis of the Taiwan Slate Belt, *Tectonics*, *14*, 322–341.

Turcotte, D. L., and G. Schubert (2002), *Geodynamics*, 2nd ed., 456 pp., Cambridge Univ. Press, New York.

Waschbusch, P. J., and L. H. Royden (1992), Spatial and temporal evolution of foredeep basins: Lateral strength variation and inelastic yielding in continental lithosphere, *Basin Res.*, *4*, 179–196.

Whipple, K. X., and B. J. Meade (2006), Orogen response to changes in climatic and tectonic forcing, *Earth Planet. Sci. Lett.*, *243*, 218–228.

Willett, S. D., D. M. Fisher, C. W. Fuller, E.-C. Yeh, and C.-Y. Lu (2003), Erosion rates and orogenic-wedge kinematics in Taiwan inferred from fission-track thermochronometry, *Geology*, *31*, 945–948.

Yeh, Y. H., et al. (1998), Onshore/offshore wide-angle deep seismic profiling in Taiwan, *Terr. Atmos. Oceanic Sci.*, *9*, 301–316.

Yu, H.-S., and Y.-W. Chou (2001), Characteristics and development of the flexural forebulge and basal unconformity of western Taiwan Foreland Basin, *Tectonophysics*, *333*, 277–291.

Yu, S.-B., H.-Y. Chen, and L.-C. Kuo (1997), Velocity field of GPS stations in the Taiwan area, *Tectonophysics*, *274*, 41–59.

Yue, L.-F., J. Suppe, and J.-H. Hung (2005), Structural geology of a classic thrust belt earthquake: The 1999 Chi-Chi earthquake Taiwan (M_w = 7. 6), *J. Struct. Geol.*, *27*, 2058–2083.

J. P. Avouac, Tectonics Observatory, California Institute of Technology, Pasadena, Mail Code 100-23, Pasadena, CA 91125, USA.

M. Simoes, Géosciences Rennes, CNRS Université Rennes 1, F-35042 Rennes Cedex, France. (martine.simoes@univ-rennes1.fr)